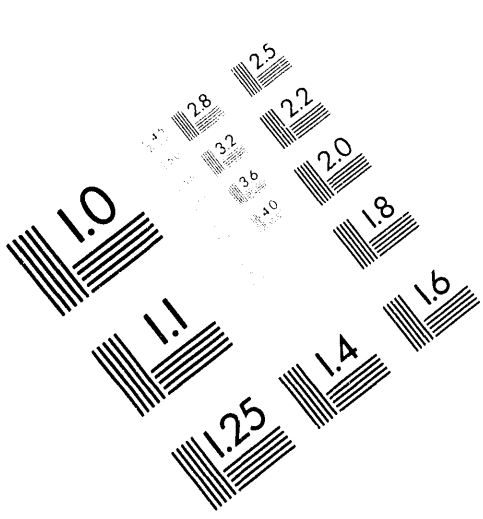

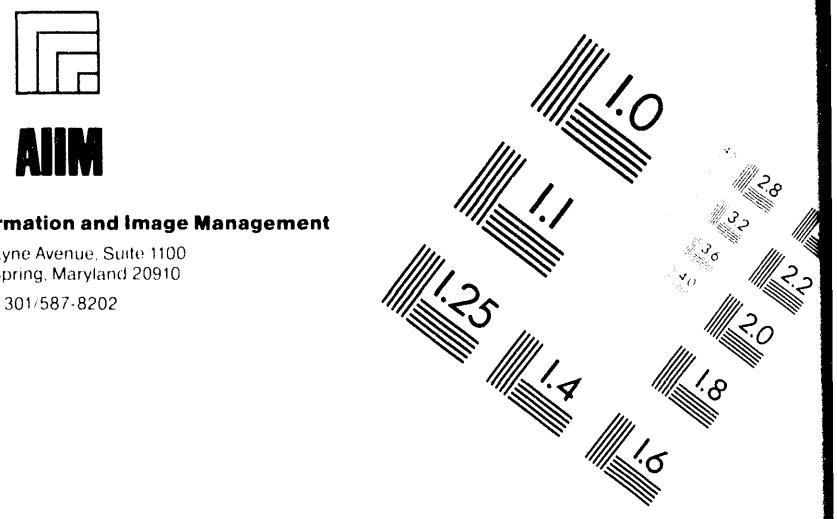

Association for Information and Image Management

1100 Wayne Avenue, Suite 1100
Silver Spring, Maryland 20910

301/587-8202

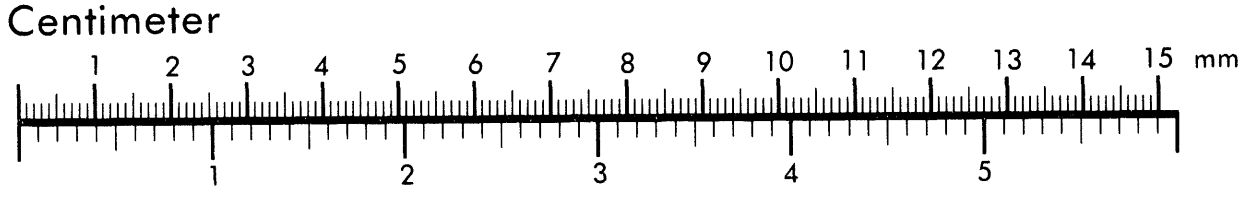

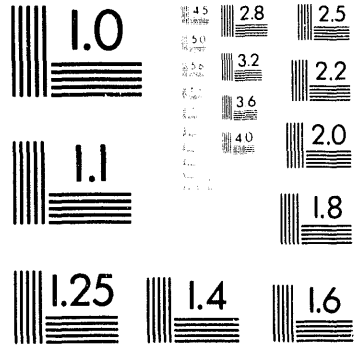

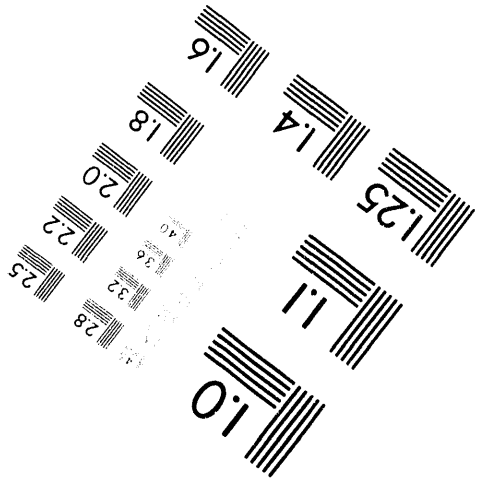

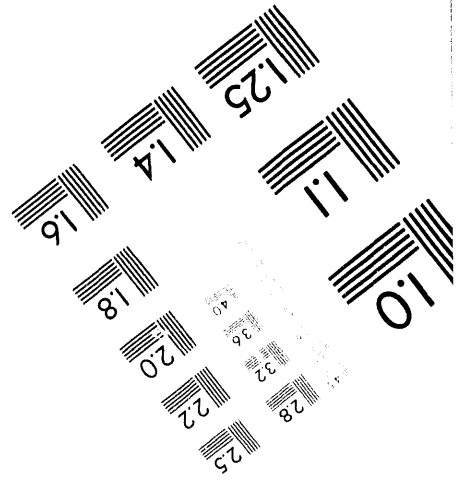

MANUFACTURED TO AIIM STANDARDS
BY APPLIED IMAGE, INC.

1 of 1

ANL/CMT/PP--78377

Ga, Ca, and 3d Transition Element (Cr through Zn) Partitioning Among Spinel-Lherzolite Phases from the Lanzo Massif, Italy: Analytical Results and Crystal Chemistry

by Roy A. Wogelius[1] and Donald G. Fraser[2]

[1]Geosciences Group, Chem. Tech. Div.,
Argonne National Laboratory CMT-205
9700 S. Cass Ave. Argonne, IL 60439;

[2]Department of Earth Sciences,
University of Oxford,
Parks Road, Oxford, OX1 3PR, England

ABSTRACT

Ultramafic rocks exposed in the Lanzo massif, Italy, preserve a detailed record of mantle geochemistry, melting, and sub-solidus re-equilibration. Plagioclase(+ spinel)-lherzolite samples were analyzed by Scanning Proton Microscopy (Oxford) and other techniques. Previous work postulated partial melting events and a two-stage sub-solidus cooling history for the massif. The present work builds on those results, noting Ga enrichment on spinel-clinopyroxene grain boundaries, high Ga and transition element content of spinel, and pyroxene zonation in Ca and Al. Trace element concentrations in olivine and orthopyroxene are also presented. Zoning trends are interpreted as being due to diffusion during cooling. Olivine-clinopyroxene Cr and Ca exchange equilibrium as well as the clinopyroxene and spinel zonation trends support the conclusion that the massif experienced at least two sub-solidus cooling episodes, one at approximately 20 kbar (to 1000°C) and one at approximately 8 kbar (to below 750°C). Furthermore, Ga concentrations in cores of Lanzo high-Cr spinels are high (82-66 ppm) relative to other mantle spinels (66-40 ppm), indicating enrichment. Ga content of ultramafic spinels apparently increases with Cr content. This may be due to either one or both of the following reasons: 1) increased solubility of Ga in the structure stemming from crystal chemical effects, 2) higher Ga activities in associated silicate melts. Thus, during melting, high-Cr residual spinel may tend to buffer the solid phase Ga concentration. These spinels are not only rich in Ga and Cr (max.=26.37 el. wt. %), but also in Fe (max=21.07 el. wt. %), Mn (max.=3400 ppm), and Zn (max.=2430 ppm). These enrichments are again due to the extraction of melt and related partitioning of these elements into the spinel structure. Low Ni (min.=1050 ppm) concentrations

are due to the unsuccessful competition of Ni with Cr for octahedral sites in the structure caused by crystal field effects. Comparisons of the change in partitioning behavior as a function of Cr content among several 3d transition elements for spinels from Lanzo and other localities allow us to separate crystal field effects from bulk chemical effects and to show, for example, that in typical mantle assemblages the inversion of the value of the olivine-spinel partition coefficient for Ni from <1 to >1 should occur at ~11% element wt. Cr in spinel.

Introduction

Earth's upper mantle is composed of a lherzolitic phase assemblage, but outcrops of lherzolite bodies are extremely rare on the earth's surface because of the difficulties involved in uplifting such high density lithologies to the surface and in preserving them once exposed. Thus, the few ultramafic massifs such as Lanzo which are exposed at the surface present a rare opportunity to study the geochemistry of intact mantle slices and also give insight into the large scale tectonic processes which created and preserved them.

The Lanzo massif is located in northwestern Italy in the inner Alpine arc near Turin, adjacent to the Ivrea zone. For a detailed structural and petrologic study see Boudier (1978). Previous studies of the Lanzo ultramafic body have determined that it has a complicated genetic history. Three fundamental facts have however been established. 1) Melt was extracted, probably during multiple events both in the spinel- and plagioclase-lherzolite field, resulting in reduction in clinopyroxene content and producing Cr- and Fe-rich spinel (Nicolas, 1986; Loubet and Allègre, 1982). Melt may also have been generated in the plagioclase stability field. Deciphering the history and nature of melt generation is complicated by the likelihood that liquid generated at depth reacted with overlying solid lherzolite during melt ascent (Boudier, 1978; Ottonello et al., 1984). 2) Sub-solidus uplift of the body occurred in at least two stages. From equilibrium in the spinel lherzolite field the massif was adiabatically uplifted to about 8 kbar pressure and

cooled to ambient temperatures (below 750 °C). This conclusion was reached by three different methods; first by Ernst (1978, 1981) from pyroxene thermometry, second by Boudier and Nicolas (1985) and Nicolas (1986) arguing from thermal structure and bulk phase relationships, and third by Wogelius and Bishop (1989) based on olivine-clinopyroxene-orthopyroxene thermobarometry. Plagioclase formed during this process, but incomplete chemical re-equilibration at intermediate depth is recorded by the presence of spinel and by chemical zoning in olivine, pyroxene, and spinel. Uplift subsequent to this intermediate pressure event finally brought the massif into the near surface environment. Shearing and extension of the massif produced foliation, re-crystallization, and a reduction in grain size (Nicolas et al., 1971). During or after the final stage of uplift, hydrothermal activity partially serpentinized the body and added another low-temperature mineral assemblage. 3) Although similar in bulk chemistry and tectonic environment, subtle trace element differences between Lanzo and the ultramafic bodies exposed nearby to the northeast (Balmuccia, Baldissero) in the Ivrea zone suggest a surprising and important difference between the modes of emplacement of Lanzo and the Ivrea ultramafics (Nicolas et al., 1971). This may be due to a departure from adiabatic conditions of uplift at greater depths for the Ivrea zone relative to Lanzo (Nicolas, 1986). The low concentrations of Ca in olivines from Baldissero and Balmuccia are consistent with slow uplift rates along a sub-adiabatic P-T path (Wogelius and Bishop, 1989).

In order to work out further details of the mode of emplacement of the Lanzo massif and to gain insight into mantle geochemistry, detailed analyses of minerals from Lanzo and from Kilbourne Hole (southwest U.S., sample supplied by B.J. Wood) were made with the Oxford Scanning Proton Microprobe (SPM) and with various electron microprobes (EMA). The Lanzo

sample discussed here was taken from the same location as sample 6 in Wogelius and Bishop (1989). The Kilbourne Hole sample was analyzed in order to compare SPM and EMA results from Lanzo with a well-characterized xenolith. In this communication spinels are highlighted because they are by far the smallest volume fraction of the solid phases present in the Lanzo lherzolite and therefore during solid state re-equilibration or during melting events compositional changes of spinels may be great. For example, Cr/(Cr+Al) may vary by a factor of 15. Trace element variation may also be large. Pressure and temperature effects on phase equilibria can be exploited as geo-thermometers and -barometers, but compositional effects must be accounted for. In addition, certain elements can act as indicators of amount of melt extracted from a system.

Lanzo spinels have a high chromite component, are low in Ni, and high in the elements Ga, Zn, and Mn. Comparison of Lanzo data with other spinel lherzolites shows that crystal field effects can play a major role during trace element partitioning into spinel as the Cr content increases, as often happens during melt extraction. This behavior can be predicted and accounted for. Furthermore, despite previous studies that suggest Ga varies directly with Al content in spinel, we show that trace amounts of Ga successfully compete with both Al and Cr for lattice sites in spinel. Variations in the Ga content of spinel are thus controlled both by whole rock bulk composition and by changes in phase equilibria.

Analytical Methods

Self-supporting thin section targets of 80 μm thick and 100 μm thick were prepared of

Kilbourne Hole and Lanzo samples, respectively. Scanning proton microscopy (SPM) of both targets was completed at the Oxford SPM facility. Analyses were performed with a 3 MeV proton beam with a beam current of approximately 200 pA. Proton induced x-ray emission (PIXE) spectra were detected with a Si(Li) energy dispersive spectrometer at detector distances between 17 and 60 mm through 2.5 mm Perspex, 1 mm Perspex and 235 μm Be filters. The incident beam was maintained at diameters of 2 μm or less. PIXE spectra were deconvoluted with both PIXAN and GEOPIXE at Oxford using the filter transmission expressions of Clayton et al. (1986) for Be and for Perspex of Grime and Wogelius (1992). Resultant concentrations were scaled with collected charge correction factors (Q_c) obtained by comparison with Rutherford backscattering spectra (RBS) and with electron microprobe analyses (EMA). For the spinel analyses presented here EMA analyses were completed as close to the SPM point analysis as was possible. Non-charge corrected PIXE results for major elements were typically within 5% of EMA.

Because of the deep penetration of the proton beam, Rutherford back scattering (RBS) spectra were also obtained using a high angle detector in order to allow "double-phase excitation" to be recognized. This occurs when significant quantities of x-rays are produced in a thin layer of a different phase overlying the phase of interest or from below the phase of interest in a buried phase. RBS spectra are sensitive to changes in stoichiometry of the target and allow the investigator to see, for example, when a spinel analysis is being interfered with by a thin overlying or underlying olivine grain. The RBS spectra also give detailed information about phase thickness and an independent check on total charge absorbed by the target specimen. Double-phase excitation is a common occurrence, especially in the sub-100 μm diameter mineral

grains for which the high lateral resolution of SPM is so useful. Without RBS analyses collected concurrent with the PIXE data extremely questionable results may be obtained.

Targets were analyzed by standard EMA wavelength dispersive spectrometry (WDS) at accelerating voltages of 20 and 15 kV. The two SPM targets were analyzed to provide a cross-check on the PIXE data. Other standard thin sections of Lanzo samples were analyzed to supplement the SPM and EMA results from the SPM target, partly to provide better statistics for thermobarometric calculations and partly to be sure that the specimen prepared for SPM analysis was not compositionally anomalous.

Trace Element Results

Spinel- Spinels from the Lanzo region exhibit high concentrations of Ga, Zn, and Mn. Figure 1 shows the pronounced Ga and Zn peaks in the PIXE EDS spectrum of a typical Lanzo spinel (K_β peaks are not labelled on Figure 1). Tables 1 and 2 summarize the EMA and SPM point analyses, respectively, of spinels from Lanzo and Kilbourne Hole. Most Lanzo spinels are extremely small, on the order of 100 μm across (maximum dimension), although one large spinel over 300 μm across was located. All six of the Lanzo spinels that were analyzed show high Cr contents (22.0 to 26.4 el. wt. % Cr), even the large spinel represented by EMA analyses 2A and 2B is not significantly different. In total, 17 point analyses of 5 different spinel grains were obtained, but because of difficulties in spectrum deconvolution only 5 point analyses are of sufficient quality to be presented as concentration measurements. However, the PIXE spectra

produced for the remaining 12 analyses are extremely similar to those used in calculating the results presented in Table 2 and support our assumption that these two spinels are representative of the spinel population in this Lanzo sample.

Very few data are available on the Ga content of spinel even though spinel is the host phase with the highest concentration of this element in the earth's mantle. Estimates of the whole earth abundance of Ga therefore rely on accurate knowledge of the average Ga concentration in spinel lherzolite. The average Ga concentration of 76 ppm in these spinels is slightly greater than the Ga contents of spinel from xenoliths from Mt. Porndon, Australia measured by McKay and Mitchell (1988). They reported concentrations of 64, 66, and 44 ppm. Whether the Lanzo samples are more typical of spinel lherzolite or are enriched relative to the average can only be concluded by gathering more data, although the Kilbourne Hole spinel Ga content of 64 ppm along with the Mt. Porndon analyses suggests that the Lanzo spinels are Ga enriched.

Figure 2 shows a comparison of the Zn, Ga, Cr, and Ca distribution between spinel, olivine, and clinopyroxene. Spinel is the high Cr phase at the center of the field of view; clinopyroxene is the high Ca phase at the bottom of the scan; olivine is the low Zn, low Ca, and low Cr region at the top of the scan. The scan was generated by rastering the proton beam over a 100 μm^2 area and recording the characteristic x-ray counts as a 256 X 256 pixel map. Concentrations are relative, with yellow areas equalling high concentration and white areas low. Note the even distribution of Zn in the spinel as compared to the Ga distribution. EMA points 1-A through 1-I and corresponding SPM points are shown on the Cr map. The spinel is slightly zoned in Fe, richer near the cpx boundary and poorer at the olivine boundary, with Mg showing the opposite trend.

A linescan along the trace indicated on Fig. 2 was also completed by SPM. Figure 3 shows the results of that scan for Ga, Ca, and Cr. The locations given on Tables 1 and 2 for spinel no. 1 correspond to the x-axis on Fig. 3. The lower part of the figure clearly shows the crossover in Ca and Cr x-ray counts in the phase boundary region between spinel and cpx. The gentle slopes of the data curves indicate that the boundary is not perpendicular to the surface, instead the cpx overlies the spinel in a thinning wedge from approximately x=10 to 30 μm. (The boundary dips 56° to the left from x=30 μm.) Along this inclined border, the upper figure indicates that the spinel is enriched in Ga by as much as a factor of six relative to the core spinel Ga concentration of 76 ppm indicated by the dashed line. Due to the complex nature of the boundary, the linescan could not be accurately calibrated. For reference, the SPM point analyses are shown as the solid circles. We believe grain boundary enrichment indicates loss of Ga from the cpx into the spinel during depressurization and cooling. Data from inclusions within diamonds shows that the partitioning of Ga between clinopyroxene and garnet is highly dependent on temperature, with K_D(cpx/gt) decreasing as temperature decreases (Griffin et al., 1988). This indicates that Ga solubility in clinopyroxene relative to garnet decreases during cooling, and that Ga diffusion from clinopyroxene into garnet would be expected. Because Ga is also compatible with the spinel lattice, we would expect the same type of behavior during cooling in a clinopyroxene-spinel system. Slight enrichment in Cr is also shown in the spinel near the cpx boundary. Cpx-spinel Ga exchange is the best explanation for this observation because we have examined ol-sp and opx-sp boundaries and do not see similar enrichment. If Ga had been deposited by a liquid phase we would expect enrichment along the entire spinel edge, not just along the clinopyroxene-spinel boundary. Figure 4 shows an example of an ol-sp boundary as

imaged by PIXE for the elements Ga, Zn, Cr, and Cu. Note the even distribution of Ga in the spinel. The high Zn-Cu phase at the center of the figure will be discussed below.

Olivine- Ca concentrations in olivine measured by SPM point analyses taken along a line from olivine rim to core increase from 400 ppm maximum at the rim to 650 ppm at the core as shown on Table 3. (Wogelius and Bishop (1989) reported zoning from 300 to 600 ppm measured by EMA.) This confirms previous work on these samples and is a result of Ca diffusing out of the olivine as the massif cooled from 1000 °C to below 750 °C at ~8 kbar (Wogelius and Bishop, 1989). Point number 126177 was taken within 50 μm of the cpx boundary. Because of the known phase boundary fluorescence effect (Adams and Bishop, 1986), no Cr or Ca concentrations are reported for olivine analyses within 50 μm of cpx or sp grains. Aside from Ca, the trace element concentrations in the olivine as measured by point analysis are fairly constant. Unfortunately, even though we experimented with count times as long as 63 minutes and various filters, because of poor counting statistics for Ga in olivine we were not able to measure the Ga concentration accurately for this phase.

Line scans were also obtained for the elements Ca, Cr, Mn, Fe, Ni, Zn, Y, and Zr across several olivine-clinopyroxene boundaries from olivine core to clinopyroxene core. No clear indication of zoning in the olivine except for the Ca profiles and some leaching of Fe and Ni along cracks was apparent. The flat Cr concentration in olivine near cpx boundaries suggests that chemical equilibrium was obtained for that component between those two phases. It should be noted that the relatively high background generated by the Fe in the olivine significantly reduced the sensitivity of the SPM linescan technique to fluctuations in the x-ray signal of lighter elements. Various filters and detector distances were experimented with, but, for example, only

by point analysis could the Ca zoning be accurately assessed.

Pyroxene-Lanzo clinopyroxenes show concave grain boundaries with olivine indicating that these clinopyroxenes have been melted (Nicolas, 1986). In contrast to the olivines, SPM linescans and EMA point analyses show that almost all Lanzo clinopyroxenes (cpx) are zoned in the major elements Ca, Al, Si, and Fe. Clinopyroxene rims are enriched in Ca and Si but depleted in Al and Fe. Figure 5 shows this variation in Ca and Al as measured by EMA on a cpx grain. EMA point analyses are represented by the large open symbols, circles for CaO, triangles for Al_2O_3. An analogous result was obtained on another cpx grain analyzed by an SPM linescan. This result is included on Figure 5 where the SPM linescan data are shown as the small filled circles which indicate a 2% increase in CaO concentration at the rim relative to the core. These major element trends are a constant feature of the Lanzo cpx. Orthopyroxene (opx) grains are also usually zoned in the Al component and may show zoning in Ca as well. Table 4 summarizes the typical core and rim pyroxene compositions measured by EMA.

Trace element concentrations for the pyroxenes as measured by SPM are shown in Table 3. Ga contents are also slightly higher for Lanzo cpx and opx than those reported by McKay and Mitchell (1988), although again the concentrations are similar (approximately 8 ppm and 5 ppm for Lanzo cpx and opx respectively versus 4 ppm and 3 ppm for the Mt. Porndon samples.) The Zn concentrations reported for opx (26-34 ppm) are similar to those reported by Kurat et al. (1980) for xenoliths from Kapfenstein, Austria (24-40 ppm). There are, in general, no large changes in trace element concentrations either between similar grains or between this population and that of an average spinel lherzolite. Clinopyroxene analyses 1-A and 1-B were taken on the same grain. SPM mapping indicated a patchy texture in the Y and Zr distribution in this cpx

which is within 50 μm of a grain boundary with olivine. To accumulate better counting statistics, point analyses were completed in the high and low concentration areas, respectively. Measurements were taken under identical conditions, but useful data for Y and Zr were produced in only one of the analyses. Thus, there may be some zonation in Y and Zr in the Lanzo cpxs but, if present, it does not mirror the Ca and Al zoning.

In the cpx the 2% Ca zonation also caused drastic shifts in background level which generated false zoning patterns for the light transition elements. This spurious result was accounted for by plotting, for example, Co counts/Ca counts. These normalized cpx linescans were flat for Cr, Mn, Fe, and Co.

Zn-Cu Accessory Phase-A point analysis was obtained of the high Zn-Cu phase shown at the center of Figure 4. The RBS spectrum for this analysis is presented as Fig. 6A. For comparison the RBS patterns obtained from chromian spinel and forsteritic olivine are also shown as Fig. 6B and 6C, respectively. Each part of the figure has two curves; the rough or noisy curve is the measured RBS data while the smooth curve represents a best fit RUMP simulation of the data. The spinel was fit by a matrix composed of $Mg_{0.5}Fe_{0.5}AlCrO_4$ and the olivine was fit by a matrix of $Mg_{1.8}Fe_{0.2}SiO_4$. Both simulations included a 20 nm thick carbon coat which appears as the small hump at 2150 keV. Single phase simulations were unable to reproduce the RBS spectrum obtained for the high Zn-Cu region. Best fit was obtained when a 1.50 μm thick layer of $(Zn,Cu)CO_3$ was simulated above a 100 μm thick layer of olivine. This result is given in Fig. 6A. Note the extremely high Zn signal and the high C signal in this spectrum. Besides those two features, the spectrum resembles the olivine RBS spectrum. This is an excellent example of the double-phase excitation discussed in the *Methods* section and demonstrates how collecting

simultaneous RBS and PIXE data adds to the analytical power of the SPM. The lack of a distinct S peak and the strong C signal indicates that this is most likely a carbonate mineral or a mixture of carbonate and oxide.

As expected, the PIXE point analysis contains a significant contribution from the underlying olivine and is therefore difficult to deconvolute. The PIXE EDS spectrum is dominated by Fe (from the olivine), Cr (mostly from fluorescence of the spinel), Zn and Cu. Assuming all of the Fe and Cr counts are contamination gives a stoichiometry of $Zn_{0.4}Cu_{0.6}CO_3$. As and S do appear as traces in the analysis with maximum concentrations of 2000 ppm and 4000 ppm, respectively. We suspect this was a sulfide that has reacted with aqueous fluids in the shallow crust to form carbonate and that the trace As and S are weathering residue. No Ga peak was noted for this phase, the lower limit of detection for Ga in this analysis being 50 ppm.

Secondary phases- The sample prepared for SPM analysis exhibited well-developed alteration along a network of cracks. Veinlets of secondary phases are as wide as 0.1 mm. X-ray diffraction and EMA identify the secondary phases as chrysotile $\{[Mg_{4.6}Fe_{0.2}Al_{1.2}][Al_{0.3}Si_{3.7}]O_{10}(OH)_8\}$ and clinozoisite $\{Ca_2Fe_{0.1}Al_{2.9}Si_3O_{12}(OH)\}$.

Discussion

Thermobarometry- Because of the Al zoning, temperature calculations for these samples using the method of Wells (1977) are quite different depending on whether core or rim pyroxene compositions are used; core temperatures tend to be approximately 1125 °C and rim temperatures

cluster around 1000°C. Tables 5 and 6 present the results of all temperature calculations. Previous work (Wogelius and Bishop, 1989) noted this zoning. Mass balance calculations show that the diffusion of Ca from olivine into cpx cannot supply enough Ca to raise the rim concentrations to the levels observed: olivine loss is a factor of five too low. Furthermore, ol-cpx exchanges cannot account for the Al profiles. Temperatures were also calculated for Cr exchange between olivine and clinopyroxene using the method of Stosch (1981), these results are also shown on Table 5. This method was calibrated with the opx-cpx Al exchange reaction and therefore is expected to show good agreement with temperatures calculated by that method, which it indeed does. Note however that neither the cpx nor the olivines are zoned in Cr content despite the persistence of zoning in other components.

Temperatures were also calculated for olivine-spinel Mg-Fe^{2+} exchange equilibrium using the method of Fabriès (1979). While a determination of the spinel Fe^{3+} content is needed to make these calculations precise, temperatures calculated with Fe^{3+} content of the spinel estimated from the electron microprobe data are, as expected, much lower than the temperatures calculated by either of the other methods. For example, the large spinel-olivine pair shown on Figure 4 give a temperature of 865°C with no significant difference if either the spinel core or rim composition is used in the calculation. A small spinel-olivine pair, with the olivine analysis taken within 30 μm of the spinel, gives a temperature of 805°C. This agrees with Fabriès' (1979) results from other ultramafic complexes, and fits in well with our postulated two-stage cooling history. The lower temperatures recorded by this thermometer are probably correlated with the low pressure cooling event recorded in the olivine Ca profiles.

Pyroxene zoning clearly must result from cooling during ascent and re-equilibration with

other Ca and Al bearing phases including spinel and silicate melt. Slow diffusion of Al and Ca in cpx left the core out of equilibrium with the rim, although cooling was fast enough to obliterate the record of the even higher temperatures the massif must have reached during the generation of melt.

Calculation of pressures from olivine-cpx Ca exchange depends explicitly on knowing the temperature of the sample. Pressure calculations must be in phase with estimated temperatures or spurious P-T relationships will result (Fraser and Lawless, 1978). Furthermore, the equilibrium thermodynamic exchange reaction as calibrated experimentally by Adams and Bishop (1986) gives pressures which are 3.8 kbar higher than pressures calculated using the empirical expression, also experimentally calibrated, of Köhler and Brey (1990). Despite the inability of this more recent work to interpret the exchange thermodynamically, the greater pressure and temperature range examined makes it useful for purposes of comparison. Given the strong temperature dependence of this reaction the errors in calculated pressure are probably at least as great as the discrepancy between the methods. Table 5 presents pressures calculated for these samples using the Adams and Bishop (1986) method, we assume errors of ±5 kbar. Pressures calculated assuming olivine cores are in equilibrium with pyroxene rims cluster around 20 kbar. If in fact the olivine cores were in equilibrium with pyroxene cores then the last equilibration pressure was slightly lower, at around 14 kbar. In either case, the two-pyroxene temperatures and pressures calculated from either the Adams and Bishop (1986) expression or the Kohler and Brey (1990) method put these samples well below the peridotite solidus in the spinel stability field or very close to the spinel-plagioclase transition pressure.

Empirical Partition Coefficients- Based on the data presented above, we have calculated partition coefficients for the trace elements Ca, Cr, Ni, Zn, and Ga between several mineral pairs and these are given in Table 7 for Lanzo spinel lherzolite. All partition coefficients were calculated for mineral pairs sharing a grain boundary. First of all note the high K_D for Ni between olivine and spinel. Both are higher than K_Ds calculated from the data of Stosch (1981), Cundari (1986), Frey and Green (1974), or Kurat et al. (1980) for similar samples. This is because of the extremely high Cr content of the Lanzo spinels. It is well known that because of the higher octahedral site preference energy of Cr (40 kcal) vs. Ni (20.6 kcal), as the Cr content of spinel increases the Ni content decreases (site preference energies are from Burns, 1970). Despite the high octahedral site preference energy of Cr, because of higher valency and large radius Cr cannot compete with Ni for the octahedral sites in olivine, and therefore the crystal chemistry causes the K_D between olivine and spinel for Ni to invert from <1 to >1 as the Cr content of the spinel rises. Mantle olivines typically have Ni contents of ~2900 ppm (± 350). Figure 7 presents a compilation of Cr and Ni data for peridotitic spinels from this study and from a number of other works. Not only does Figure 7 clearly show the strong correlation of spinel Ni content on Cr concentration, it also indicates that the shift in the sense of the olivine-spinel partition coefficient will occur at approximately 11% Cr element weight in the spinel.

Figures 8, 9, and 10 present similar data for Co, Mn, and Fe for a number of peridotitic spinels. The dashed lines, as on Figure 7, are least squares regression lines through the data. Regression lines for these data have been calculated without the Lanzo measurements as part of the population. This was done because of the obvious enrichment in Mn and Fe shown by the Lanzo spinels when compared to the other analyses. Fe^{+2} and Co^{+2} have low octahedral site

preference energies and Mn^{+2} has zero, so that these cations are compatible with the tetrahedral spinel site. Hence these cations would not be expected to show a negative correlation with Cr content as indeed they do not. Figure 11 shows the dependence of the slopes of the trace element vs. Cr content regression lines on the octahedral site preference energy for the respective cations. The slopes were calculated on a mole ratio scale for this figure. Knowledge of this dependence allows the crystal chemical effects to be subtracted from trace element trends for peridotitic spinels, revealing other dependencies. Thus, the high Mn and Fe contents shown on Figures 9 and 10 for the Lanzo spinels suggests these samples have been enriched relative to average spinel in spinel lherzolite by a change in the bulk chemistry of the system. Partial melt extraction is a likely candidate. On Fig. 10 the two Lanzo analyses by Boudier (1978), shown as the open circles enclosing crosses, suggest Fe enrichment in the spinels may be characteristic of the massif and part of a continuous process instead of the result of extreme fractionation. The Zn datum on Figure 11 was calculated using Lanzo data only.

Due to the grain boundary enrichment in Ga noted above we are also interested in the behavior of Ga^{+3} as a function of Cr content. McKay and Mitchell (1988) determined that mineral Ga content in garnet and spinel lherzolites is directly proportional to Al content, and that Ga enters the octahedral site in spinel. Their latter conclusion was in opposition to that of Vincent and Nightingale (1974) who suggested that Ga in spinel structures entered the tetrahedral site. It is well documented that Ga^{3+} is compatible with the spinel tetrahedral site (Hill et al., 1979), especially in the presence of cations with high OSPE (Greenwald et al., 1954). Ga^{3+} also can substitute into the octahedral site (Hill et al. 1979). Figure 12 shows the weak positive correlation between Ga and Cr content in spinels from Lanzo, Kilbourne Hole, and Mt. Porndon. Cr, Ga, and

Al are all trivalent, but Cr and Ga have identical ionic radii (0.70 Å) when in octahedral coordination. This is nearly 15% larger than the Al radius in 6-fold coordination (0.61 Å). It is logical that as the Cr content of the spinel increases, the octahedral site swells and Ga becomes more compatible. But, because Ga has zero stabilization of its electronic configuration in octahedral coordination as Cr does, as Cr concentrations rise and begin to saturate the 6-fold sites the advantage gained by Ga^{3+} through the increase in site size is diminished. However, as Cr replaces Al the spinel oxygen parameter (u) decreases, and as it decreases the tetrahedral site should contract (O'Neill and Navrotsky, 1983). Thus, because the ionic radius of Ga^{3+} in tetrahedral coordination (0.47 Å) is smaller than Mg^{2+} (0.585 Å), Fe^{3+} (0.485 Å), or any of the 3d transition metals in divalent oxidation states (0.565 to 0.655 Å), Ga occupancy of the tetrahedral site may be favored by the compression of that site due to increasing Cr content. (Ionic radii for cations in spinel are from O'Neill and Navrotsky, 1983). We therefore suggest that both expansion of the octahedral site and compression of the tetrahedral site by increasing Cr content makes the spinel structure more able to accept Ga. As Cr concentrations become extreme and severely limit the availability of 6-fold sites, Ga is successfully able to partition into the 4-fold sites, although some type of coupled substitution is required to maintain charge balance. This is a small data set and we think more data will confirm this hypothesis as well as place better constraints on the whole earth concentration of Ga. Figure 12 is clearly not consistent with a negative correlation between Cr and Ga. Note also that Smith et al. (1991) observed a positive correlation between Cr and Ga concentrations in garnets from two different garnet peridotite xenoliths.

Conclusions

Mode of Emplacement-These results corroborate earlier conclusions about the last equilibration conditions of and P-T trajectory followed by the Lanzo massif. Adiabatic uplift caused the massif to cross the lherzolite solidus in the spinel field, generating a few percent partial melt. Modal proportion of clinopyroxene decreased and residual spinels became enriched in Cr, Ni, Mn, Zn, and Fe. As the massif cooled, olivine Ca compositions became reset at this new pressure, and pyroxene compositions adjusted. A second stage of fairly rapid (adiabatic?) uplift placed the massif at shallow depth in the plagioclase field, but still out of thermal equilibrium. During isobaric cooling at this depth a number of concentration profiles were frozen in as various blocking temperatures were reached. First, diffusion profiles of Ga and Cr into spinel from cpx and of Al out of cpx were created, frozen at approximately 1000°C, the temperature recorded in pyroxene rims. Then, Ca profiles in cpx and finally Ca profiles in olivine were frozen with diffusion essentially having no effect below 750°C.

Comparison with other Peridotites-High concentrations of transition metals in spinel, coupled with extreme Ga enrichment in spinel at cpx-sp boundaries are unique features of these samples. Figure 13 compares the Cr/(Cr+Al) vs. Mg/(Mg+Fe) molar ratios of Lanzo spinels with trends measured in other peridotites. A regression of the data presented in Wood and Virgo (1989) for spinels in xenoliths from a number of localities is shown as the dashed line. Data presented by Woodland et al. (1992) for the Ronda massif are summarized as the two solid regression lines. The portion of the line with high negative slope is derived mostly from samples

without plagioclase, the other segment is derived solely from samples that do contain plagioclase. The break in slope is interpreted as being caused by equilibration of most plagioclase-bearing samples at lower temperature (Woodland et al., 1992), an interpretation consistent with phase equilibria. Also shown on Fig. 13 are the data from Lanzo given by Boudier (1978, hollow symbols) and from this study (solid symbols) for Lanzo and Kilbourne Hole. Circles are plagioclase-bearing lherzolite, triangles are spinel lherzolite, dunite, or websterite, and squares are ariegite. The single diamond labeled KH is the Kilbourne Hole sample which falls well within the range of values measured by Wood and Virgo (1989) for Kilbourne Hole spinels. All data have been displayed with Fe as total Fe to remove any effects from inaccurate assessment of the Fe^{3+} content among the various data sets. Note the similarity between the trend displayed by the Lanzo samples and the trend displayed by the samples from Ronda. The relatively flat trend exhibited by spinels from Lanzo plagioclase-lherzolite, when compared with the data from Ronda and from xenoliths, suggests that the sub-solidus equilibration of the Lanzo massif occurred in two steps thus generating two spinel trends. Wells (1977) temperatures for the Ronda plagioclase-lherzolites (Woodland et al., 1992) are approximately 930°C, similar to the Lanzo pyroxene rim temperatures, and the olivine-spinel Mg-Fe^{2+} temperatures of 805-870°C at Lanzo are also extremely similar to the temperature of 828°C calculated for rocks from the margin of the Ronda massif. The extremely Cr and Fe rich spinels in the Lanzo plagioclase-bearing samples therefore probably formed under pressure and temperature conditions similar to those under which the less evolved spinels from Ronda formed.

Lanzo spinels, even those that are low-Cr, tend to be higher in Fe and Mn than other peridotitic spinels. Almost all samples shown on Figure 13 are more extreme in Fe content than

the xenolith or Ronda regression lines. This may be due to mass transfer between the Lanzo spinels and high-Fe silicate liquids generated at depth. Ariegite spinel compositions are extremely Cr-poor, and suggest that at least the spinel phase in this facies was formed from, or equilibrated with, low-Cr high-Fe silicate liquids as well.

Gallium in the Mantle-Based on the above results we suggest that high-Cr spinel acts as a Ga buffer in the upper mantle. The incompatibility of Ga is directly controlled by spinel composition, such that as more melt is generated or plagioclase formed driving more Cr into the spinel structure, spinel lherzolite becomes more efficient at retaining Ga and inhibits Ga loss during melt extraction. For example, whole rock analyses from Ronda (Frey et al., 1985) show that even with on the order of 30% melt extraction, concentrations of "incompatible" Ga from 0.5 to 1.0 ppm persist. This is only slightly lower than the average mantle Ga concentration of 1.9 ppm (±0.7) as calculated by McKay and Mitchell (1988).

ACKNOWLEDGEMENTS

The authors would like to thank the Oxford proton microprobe unit for all of their help, especially Geoff Grime, Mike Marsh, Judy Lansberg, Phil King, and Frank Watt. Alan Woodland, Andrew Jephcoat, and Neil Sturchio provided insightful discussions. Norman Charnley and Phil Jackson at Oxford and Steve Lane at Bristol gave technical assistance in EMA analysis and sample preparation. The analytical work was supported by NERC grant GR3/7342 to DGF; the manuscript was prepared at Argonne National Laboratory with the support of the Geosciences Research Program, Office of Basic Energy Sciences, U.S. Department of Energy under contract W-31-109-Eng-38.

REFERENCES

ADAMS G.E. and BISHOP F.C. (1986) The olivine-clinopyroxene geobarometer: experimental results in the CaO-FeO-MgO-SiO_2 system. *Contrib. Mineral. Petrol.* **94**, 230-237.

BOUDIER F. (1978) Structure and petrology of the Lanzo peridotite massif (Piedmont Alps). *Geol. Soc. Amer. Bull.* **89**, 1574-1591.

BOUDIER F. and NICOLAS A. (1985) Harzburgite and lherzolite subtypes in ophiolitic and oceanic environments. *Earth Planet. Sci. Letters* **76**, 84-92.

BURNS R.G. (1970) *Mineralogical applications of crystal field theory.* Cambridge Press.

CLAYTON E.J. (1986) PIXAN-the Lucas Heights PIXE analysis package. *Australian Atomic Energy Commission Report;* AAEC-M113.

CUNDARI A., DAL NEGRO A., PICCIRILLO E.M., DELLA GIUSTA A., and SECCO L. (1986) Intracrystalline relationships in olivine, orthopyroxene, clinopyroxene, and spinel from a suite of spinel lherzolite xenoliths from Mt. Noorat, Victoria, Australia. *Contrib. Mineral. Petrol.* **94**, 523-532.

ERNST W.G. (1978) Petrochemical study of lherzolitic rocks from the Western Alps. *J. Petrology* **19**, 341-392.

ERNST W.G. (1981) Petrogenesis of eclogites and peridotites from the Western and Ligurian Alps. *Am. Mineral.* **66**, 443-472.

FABRIÈS, J. (1979) Spinel-olivine geothermometry in peridotites from ultramafic complexes.

Contrib. Mineral. Petrol. **69**, 329-336.

FRASER D.G. and LAWLESS P.J. (1978) Palaeogeotherms: implications of disequilibrium in garnet lherzolite xenoliths. *Nature* **273**, 220-222.

FREY F.A. and GREEN D.H. (1974) The mineralogy, geochemistry and origin of lherzolite inclusions in Victorian basanites. *Geochim. Cosmochim. Acta* **38**, 1023-1059.

FREY F.A., SUEN C.J., and STOCKMAN H.W. (1985) The Ronda high temperature peridotite: geochemistry and petrogenesis. *Geochim. Cosmochim. Acta* **49**, 2469-2491.

GREENWALD S., PICKART S.J., and GRANNIS F.H. (1954) Cation distribution and *g* factors of certain spinels containing Ni^{++}, Mn^{++}, Co^{++}, Al^{+++}, Ga^{+++}, and Fe^{+++}. *Jour. Chem. Phy.* **22**, 1597-1600.

GRIFFIN W.L., JAQUES A.L., SIE S.H., RYAN C.G., COUSENS D.R., and SUTER G.F. (1988) Conditions of diamond growth: a proton microprobe study of inclusions in West Australian diamonds. *Contrib. Mineral. Petrol.* **99**, 143-158.

GRIME G.W. and WOGELIUS R.A. (1992) Solid angle dependence of transmission factor for x-ray filters used in PIXE analysis (in prep.).

KÖHLER T.P. and BREY G.P. (1990) Calcium exchange between olivine and clinopyroxene calibrated as a geothermobarometer for natural peridotites from 20-60 kb with applications. *Geochim. Cosmochim. Acta* **54**, 2375-2388.

KURAT G., PALME H., SPETTEL B., BADDENHAUSEN H., HOFMEISTER H., PALME C., and WÄNKE H. (1980) Geochemistry of ultramafic xenoliths from Kapfenstein, Austria: evidence for a variety of upper mantle processes. *Geochim. Cosmochim. Acta* **44**, 45-60.

HILL R.J., CRAIG J.R., and GIBBS G.V. (1979) Systematics of the spinel structure type.

Phy. Chem. Minerals **4**, 317-339.

LOUBET M. and ALLÈGRE C.J. (1982) Trace elements in orogenic lherzolites reveal the complex history of the upper mantle. *Nature* **298**, 809-814.

MCKAY D.B. and MITCHELL R.H. (1988) Abundance and distribution of gallium in some spinel and garnet lherzolites. *Geochim. Cosmochim. Acta* **52**, 2867-2870.

NICOLAS A. (1986) A melt extraction model based on structural studies in mantle peridotites. *J. Petrology* **27**, 999-1022.

NICOLAS A., BOUCHEZ J.L., BOUDIER F., and MERCIER J.C. (1971) Textures, structures and fabrics due to solid state flow in some European lherzolites. *Tectonophysics* **12**, 55-86.

O'NEILL H. St. C., and NAVROTSKY A. (1983) Simple spinels: crystallographic parameters, cation radii, lattice energies, and cation distribution. *Am. Mineral.* **68**, 181-194.

OTTONELLO G., ERNST W.G., and JORON J.L. (1984) Rare earth and 3d transition metal geochemistry of peridotitic rocks: I. Peridotites from the western Alps. *J. Petrology* **25**, 343-372.

SMITH D., GRIFFIN W.L., RYAN C.G., and SIE, S.H. (1991) Trace-element zonation in garnets from The Thumb: heating and melt infiltration below the Colorado Plateau. *Contrib. Mineral. Petrol.* **107**, 60-79.

STOSCH H.G. (1981) Sc, Cr, Co and Ni partitioning between minerals from spinel peridotite xenoliths. *Contrib. Mineral. Petrol.* **78**, 166-174.

VINCENT E.A. and NIGHTINGALE G. (1974) Gallium in rocks and minerals of the Skaergaard intrusion. *Chem. Geol.* **14**, 63-73.

WELLS P.R.A. (1977) Pyroxene thermometry in simple and complex systems. *Contrib. Mineral. Petrol.* **62**, 129-139.

WOGELIUS R.A. and BISHOP F.C. (1989) Subsolidus emplacement history of the Lanzo massif, northern Italy. *Geology* **17**, 995-999.

WOOD B.J. and VIRGO D. (1989) Upper mantle oxidation state: ferric iron contents of lherzolite spinels by ^{57}Fe Mössbauer spectroscopy and resultant oxygen fugacities. *Geochim. Cosmochim. Acta* **53**, 1277-1291.

WOODLAND A.B., KORNPROBST J., and WOOD B.J. (1992) Oxygen thermobarometry of orogenic lherzolite massifs. *J. Petrology* **33**, 203-230.

Table 1. EMA Point Analyses (El. Wt. %) of Lanzo (Pts. 1-6) and Kilbourne Hole (Pt. 7) Spinels

EMA Pt.*	Mn	Fe	Ni	Zn	Cr	Al	Mg	Si	Ti	x(μm)	ΣM**
1 A	0.28	19.57	0.16	0.12	24.36	14.00	6.19	0.08	0.25	36.9	3.0493
1 B	0.30	17.81	0.13	0.14	25.19	14.25	6.83	0.02	0.27	42.2	3.0427
1 C	0.34	19.06	0.14	0.13	24.49	14.08	6.04	0.02	0.24	47.6	3.0443
1 D	0.29	18.27	0.16	0.16	25.03	14.30	6.47	0.03	0.25	52.9	3.0397
1 E	0.27	18.75	0.12	0.17	25.12	14.28	6.00	0.01	0.23	58.3	3.0353
1 F	0.32	21.07	0.11	0.23	24.52	14.13	5.03	0.01	0.25	63.6	3.0417
1 G	0.29	17.39	0.17	0.08	25.33	14.58	7.12	0.01	0.26	74.3	3.0413
1 H	0.19	16.18	0.14	0.15	25.49	14.75	7.62	0.02	0.23	79.6	3.0380
1 I	0.22	16.02	0.15	0.09	25.24	14.52	7.54	0.01	0.25	85.0	3.0387
2 A	0.24	14.48	0.17	0.11	24.18	15.51	9.01	0.03	0.29	-	3.0471
2 B	0.23	14.69	0.14	0.12	24.34	15.54	9.08	0.01	0.30	-	3.0511
3	0.32	19.41	0.11	0.21	23.87	14.26	6.94	0.26	0.25	-	3.0586
4	0.23	15.81	0.13	0.23	22.85	16.37	8.35	0.05	0.19	-	3.0469
5	0.34	18.32	0.10	0.21	26.37	12.79	7.23	0.36	0.32	-	3.0574
6	0.18	16.39	0.13	n.a.	24.71	15.99	7.73	0.02	-	-	3.0326
7	0.10	9.66	0.24	0.02	14.58	24.26	12.48	0.03	0.03	-	3.0401
2σ	0.03	0.20	0.02	0.04	0.25	0.07	0.07	0.02	0.03	-	-

* Pts. 1-A through 1-I are from point scan across a single spinel. Pts. 2-A and 2-B are core and rim of single grain, respectively. Pt. nos. are cross-referenced to SPM analyses on Table 2.

** Sum of cations relative to 4 oxygens.

Table 2. SPM Point Analyses (ppm) of Lanzo and Kilbourne Hole Spinel

Pt. no.[1]	EMA Pt.[2]	Ga	Fe[3] (el. wt. %)	Ni	Zn	Cr (el. wt. %)	x(μm)	% Error[4]
175025	1 A	66 ±18	19.6	1054	2182	25.4	37.5	4
175017	1 C	75 ± 6	19.1	1133	2047	26.2	46.0	7
141040	1 E	82 ± 7	18.1	1076	1942	22.9	61.0	9
175016	1 F	81 ± 8	21.1	1090	2429	22.05	63.0	10
187026[5]	2 A	81 ±15	14.5	1156	1105	23.5	-	3
175020	7	64 ± 7	9.7	2690	699	15.6	-	7

[1] All are Lanzo except 175020.

[2] EMA pt. no. refers to point analysis on Table 1.

[3] All analyses use Fe concentration determined by EMA as internal standard except 141040 which is standardless.

[4] For all elements except Ga.

[5] Also measured for run 187026; Ca= 374, Ti= 3106, and V= 1175.

Table 3. SPM Point Analyses (ppm) of Lanzo Silicates

3a. Olivine (Fe as internal standard)

Pt. no.	Mn	±	Ni	±	Zn	±	Cr	±	Ca	±	x* (μm)
126177 A	1494	31	3802	27	31	7	**	-	**	-	31
126178 A	1505	44	3134	25	46	8	76	29	510	15	85
126179 A	1421	30	3082	25	46	8	74	30	504	15	136
126180 A	1391	29	3105	25	54	8	64	44	504	15	199
126181 A	1400	25	2989	24	39	8	40	36	563	15	257
126182 A	1412	25	3064	25	47	7	64	8	536	15	312
126183 A	1399	29	2989	24	39	7	70	56	594	14	363
126184 A	1411	27	3011	24	49	7	73	65	604	15	394
126185 A	1402	27	2963	24	48	7	79	9	635	15	499
141031 B	1203	17	2840	20	40	7	97	5	507	12	-
141032 B	1221	21	3048	34	53	14	87	14	560	18	-
141034 C	2098	168	3139	31	60	7	-	-	-	-	-
141037 D	2223	246	3046	43	51	9	-	-	-	-	-
187011 E	1210	12	2707	27	32	4	114	5	267	8	-
187031 F	1141	11	3603	36	26	5	-	-	329	10	-

*Analyses 126177-126185 are point analyses along line on single olivine grain from clinopyroxene boundary at x=0 to olivine core. 126176 is corresponding clinopyroxene analysis.

**Affected by grain boundary fluorescence.

3b. Orthopyroxene (Fe as internal standard)

Pt. no.	Mn	±	Ni	±	Zn	±	Cr	±	Ca(el. wt.%)	±	Ga	±	Ti	±	V	±
187008 A	1290	13	760	8	34	2	5711	57	1.82	0.01	<4	-	3489	35	165	5
187010 B	1204	12	735	7	32	3	5123	51	1.03	0.01	5	3	1120	11	157	6
187033 C	1261	12	830	17	26	9	4924	49	1.16	0.01	<12	-	901	18	147	19

3c. Clinopyroxene (Standardless)

Pt. no.	Mn	±	Fe (el. wt.%)	±	Ni	±	Zn	±	Cr	±	Ga	±	Y	±	Zr	±	Cu	±
141036 A	729	46	2.56	0.01	362	7	14	2	8660	129	6	1	-	-	-	-	10	2
141038 A	1184	52	2.50	0.01	351	9	16	2	8480	153	6	1	13	1	7	1	11	3
126176 B	1009	22	2.64	0.01	254	13	-	-	8529	26	10	4	-	-	-	-	-	-

Table 4. Representative EMA Analyses of Lanzo Silicates

Oxide	1A*Ol. Core	1A Opx Rim	1A Cpx Rim	1B Opx Core	1B Cpx Core	1S Opx Rim	1S Cpx Rim
SiO_2	41.92	55.61	50.77	54.68	50.19	55.29	51.79
TiO_2	-	-	-	-	-	0.17	0.38
Al_2O_3	0.07	2.67	3.68	2.75	4.65	2.10	3.75
Cr_2O_3	0.00	0.76	1.32	0.73	1.41	0.56	1.31
FeO	9.48	6.38	2.93	6.70	3.88	6.37	2.98
MnO	0.15	0.17	0.08	0.16	0.12	0.20	0.10
MgO	47.72	33.02	16.48	32.74	17.52	34.79	17.48
NiO	0.39	0.11	0.03	0.10	0.11	0.08	0.06
CaO	0.08	1.58	22.97	1.51	20.17	1.16	21.12
Na_2O	0.03	0.04	0.35	0.03	0.29	0.04	0.37
ZnO	-	-	-	-	-	0.03	0.02
Total	99.85	100.33	98.72	99.39	98.33	100.79	99.36

*Samples A and B are standard thin sections, S is proton probe mount analyzed with EMA.

Table 5. Opx-Cpx Temperature and Ol-Cpx Pressure Calculations, Lanzo Massif

Opx-Cpx (°C) Al exchange Temp.	Ol-Cpx (Kbar) Ca exchange Pres.	Cpx Quad. Comp.	Sample No., Position
950	15	0.950	1B, Rim
1060	22	0.922	1A, Rim
1060	13	0.934	1S, Rim
1121	28	0.939	1A, Core
1135	24	0.934	1S, Core
1120	24	0.924	1B, Core

Table 6. Ol-Cpx Temperatures, Lanzo Massif

Ol-Cpx (°C) Cr exchange Temp.	Ol Cr content (ppm)	Cpx Cr content (ppm)
996	97	8480
979	87	8660
949	67	8529

Table 7. Lanzo Empirical Partition Coefficients

Pair	Ca	Cr	Ni	Zn	Ga
cpx-sp	3.93×10^{2}	3.4×10^{-2}	0.34	8.24×10^{-3}	9.10×10^{-2}
			0.31	5.76×10^{-3}	7.32×10^{-2}
ol-sp	0.88	1.0×10^{-3}	3.12	4.35×10^{-2}	$<5.0\times10^{-2}$
			2.39	2.35×10^{-2}	
opx-sp	83.0	1.44×10^{-2}	0.60	0.14	6.6×10^{-2}
ol-cpx	3.64×10^{-3}	9.26×10^{-3}	14.97	4.29	< 0.67
	1.67×10^{-3}	4.69×10^{-3}	11.67	2.50	
		11.44×10^{-3}	8.94		
		10.05×10^{-3}	7.85		
			15.0		
ol-opx	6.74×10^{-2}	2.23×10^{-2}	3.68	0.97	< 1.0
		2.00×10^{-2}	3.56	1.00	
		4.77×10^{-2}	4.34		
			4.33		

Figure 1. EDS spectrum produced by PIXE point analysis of Lanzo spinel. The small squares are the raw data in $\log_{10}$ counts per channel vs. energy in keV. Dotted line is the background fit while the solid line is the fit to the data. Note the distinct Ga and Zn peaks.

Figure 2. 100 μm^2 PIXE map of Lanzo lherzolite showing (from top left clockwise) the Zn, Ga, Cr, and Ca distribution. High-Cr phase at center is spinel, high-Ca phase at lower right is clinopyroxene, low-Cr low-Ca phase at upper left and right is olivine. Note the concentration of Ga at the sp-cpx boundary and the even distribution of Zn in the spinel. The circles on the Cr map indicate the SPM point analysis locations listed on Table 2 and the solid line indicates the position of the linescan presented on Figure 3.

Figure 3. PIXE linescan across the cpx-spinel-olivine region. Upper diagram shows Ga zoning, lower diagram shows Ca (open circles) and Cr (filled circles) zonation. Note the high concentration of Ga in the inter-phase region between cpx and spinel.

Figure 4. 250 μm^2 PIXE map of another olivine-spinel boundary showing the distribution of Ga, Zn, Cr, and Cu. Spinel is the high Cr region to the right. No Ga enrichment is seen at this boundary. Note the small high-Zn and high-Cu phase present at the center of the scan.

Figure 5. Comparison of SPM to EMA data for Lanzo clinopyroxenes. The small, connected and filled circles are PIXE data from a linescan across a Lanzo cpx, the open symbols are EMA analyses at five points along a traverse from an olivine-cpx boundary inward. Open circles are CaO, open triangles are Al_2O_3 (The Al_2O_3 data has been inverted and placed on the opposite half of the linscan in order to show the compositional trends more clearly. There is a compositional mirror plane running down the center of the cpx grain for Al and Ca. This Ca-enriched Al-depleted rim is a ubiquitous feature of Lanzo clinopyroxenes.

Figure 6. RBS spectra from point analyses of Lanzo minerals. a) High Zn and Cu phase from Fig. 4. b) Spinel. c) Olivine. RBS data is the jagged line, best fit to the data is the smooth curve. RBS data fit identifies the unknown as $Zn_{0.4}Cu_{0.6}CO_3$.

Figure 7. Negative correlation observed for mantle spinels between Ni and Cr concentration. Dashed line is least squares regression line for all data. Symbols are as follows: this study-Lanzo, solid circles are SPM data, open circles EMA; Kilbourn Hole, solid diamond by SPM. Other analyses- open circles with small x are for Lanzo from Boudier (1978), open diamonds are for Kilbourn Hole from Wood and Virgo (1989), hexagons from Kurat et al. (1980), downward pointing triangles from Stosch (1981), upward pointing triangles from Wood and Virgo (1989) for other locales, squares from Frey and Green (1974).

Figure 8. Co vs. Cr compositional trend for mantle spinels. Symbols same as previous.

Figure 9. Mn vs. Cr compositional trend for mantle spinels. Regression line calculated without Lanzo analyses in data set. Note significant enrichment of Lanzo spinels in Mn relative to other

locales.

Figure 10. Fe vs. Cr compositional trend. Again note the enrichment of Lanzo spinels in Fe. Boudier's (1978) data are also above the regression line and suggest that the Lanzo massif's Fe enrichment may not be the product of extreme fractionation but may be due to early-stage enrichment during emplacement.

Figure 11. Dependence of the slope of a transition metal's molar concentration as a function of Cr molar concentration in spinel on the transition metal's octahedral site preference energy (in kcal). Solid symbols are calculated from the data presented above, the open symbol predicts a value for Cu.

Figure 12. Spinel Ga concentration as a function of Cr concentration. A positive correlation is indicated by the data. Symbols same as previous except open squares- McKay and Mitchell (1988).

Figure 13. A comparison of the Lanzo spinel major element chemistry to that of other mantle spinels. Dashed line is a regression of the data presented by Wood and Virgo (1989) for spinels from various locations, solid line is calculated from the data of Woodland et al. (1992) for spinels from the Ronda massif. Woodland et al. (1992) interpret the compositional kink as being due to spinel formation at two different temperatures. The compositional trend exhibited by the Lanzo samples are similar and thus consistent with two periods of spinel growth at distinct temperatures. In addition the comparison highlights the extreme Fe and Cr enrichment exhibited by these spinels. The diamond labeled KH represents our measurement of Kilbourn Hole spinel.

Oxford University SPM Facility

Run 141.040 OES105 Lanzo L1

t: 0:19:03 Beam Q: 0.1627uC

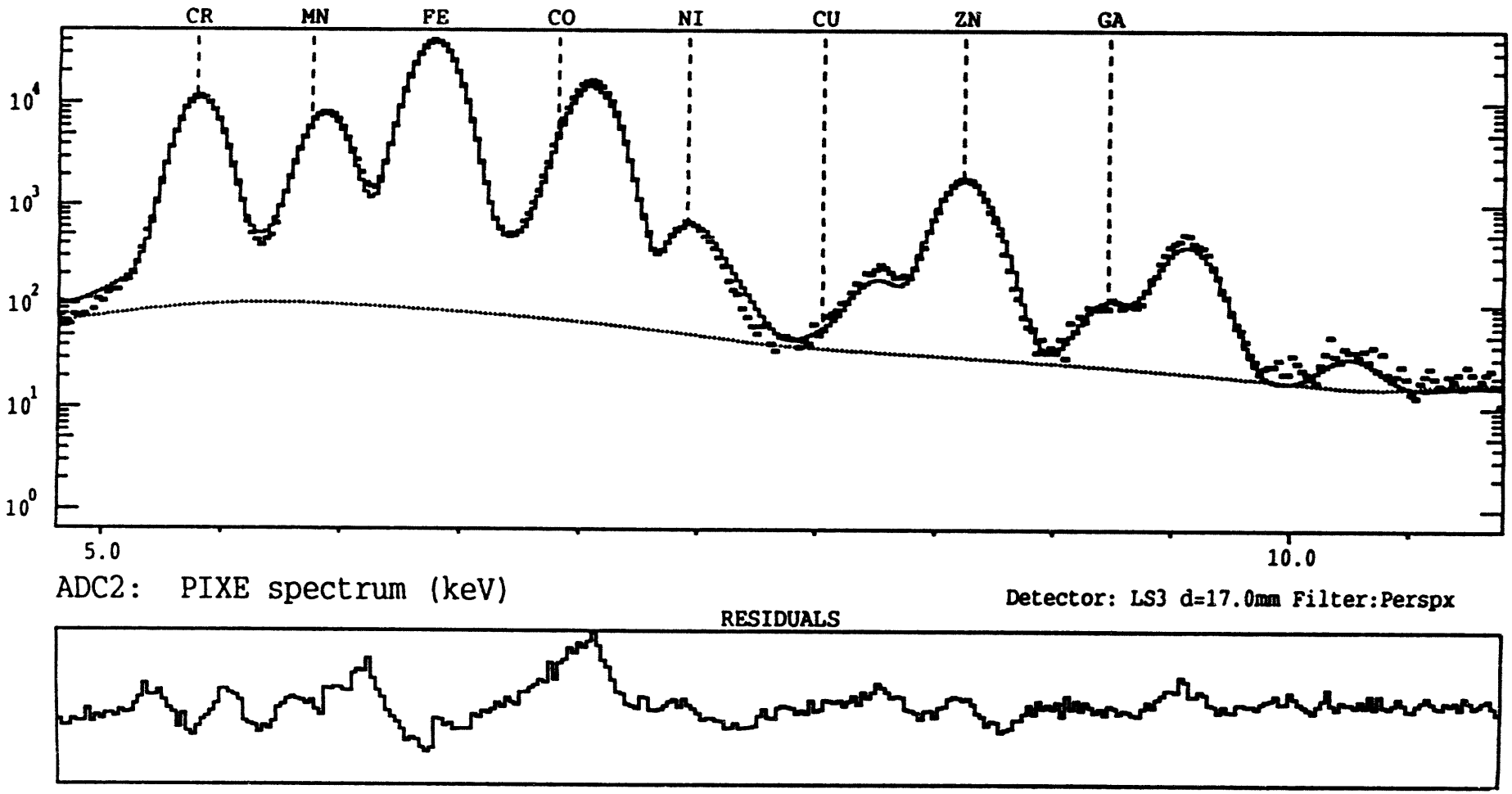

Fig 1

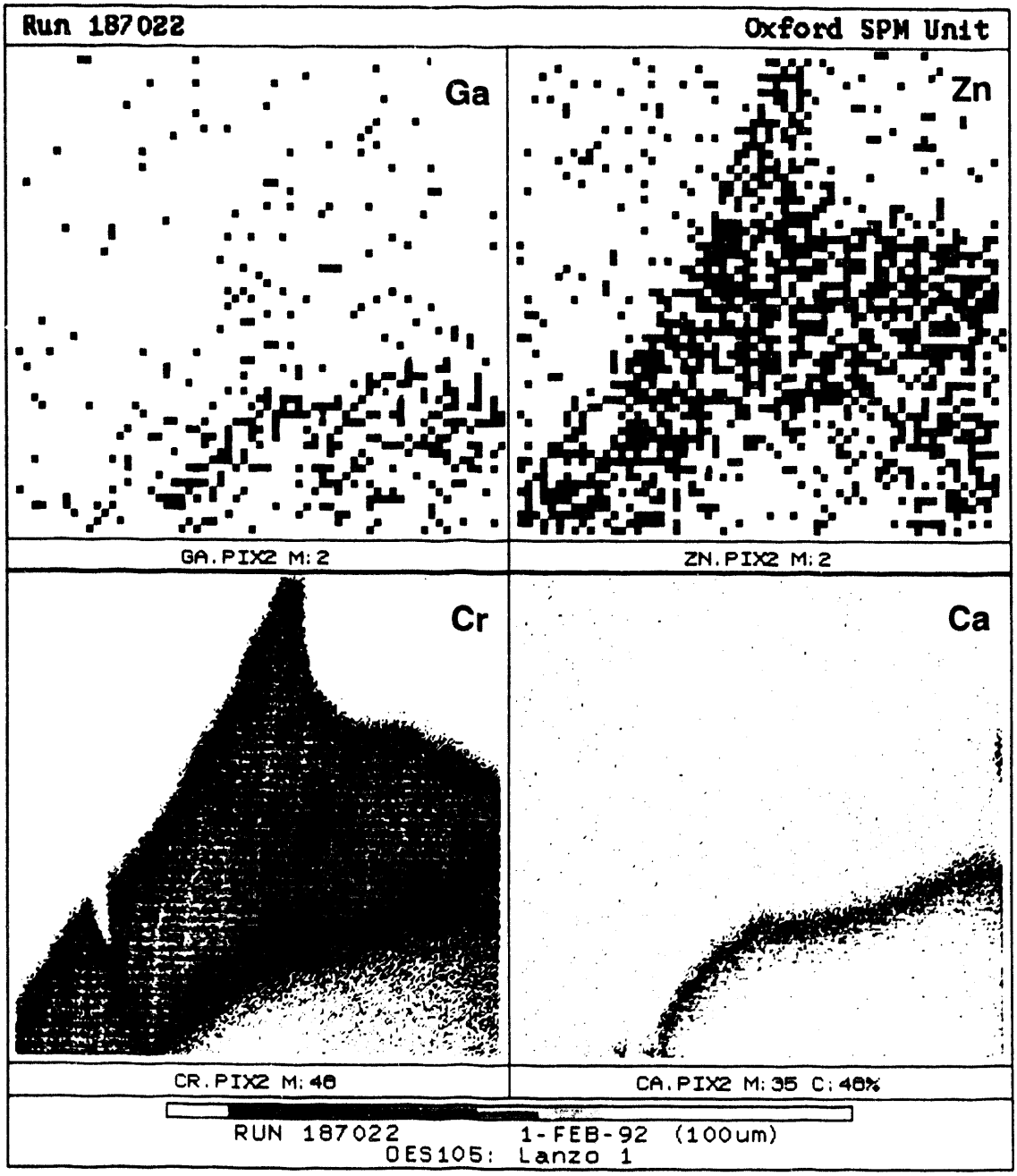
Run 187022
Oxford SPM Unit
Ga
Zn
GA.PIX2 M:2
ZN.PIX2 M:2
Cr
Ca
CR.PIX2 M:46
CA.PIX2 M:35 C:46%
RUN 187022 1-FEB-92 (100um)
OES105: Lanzo 1

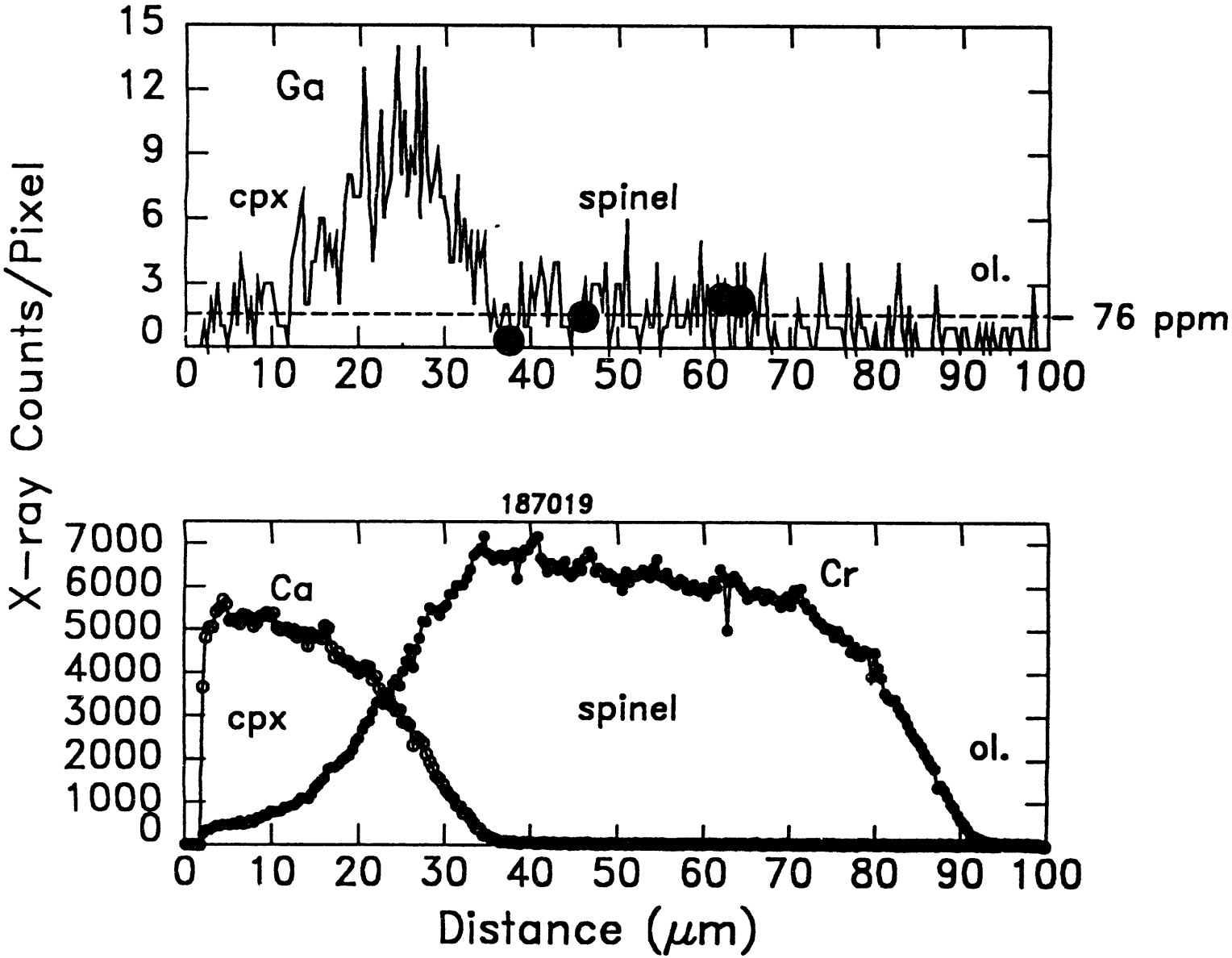
15
12
9
6
3
0
Ga
cpx
spinel
ol.
76 ppm
0 10 20 30 40 50 60 70 80 90 100
187019
7000
6000
5000
4000
3000
2000
1000
0
Ca
Cr
cpx
spinel
ol.
0 10 20 30 40 50 60 70 80 90 100
X-ray Counts/Pixel
Distance (μm)

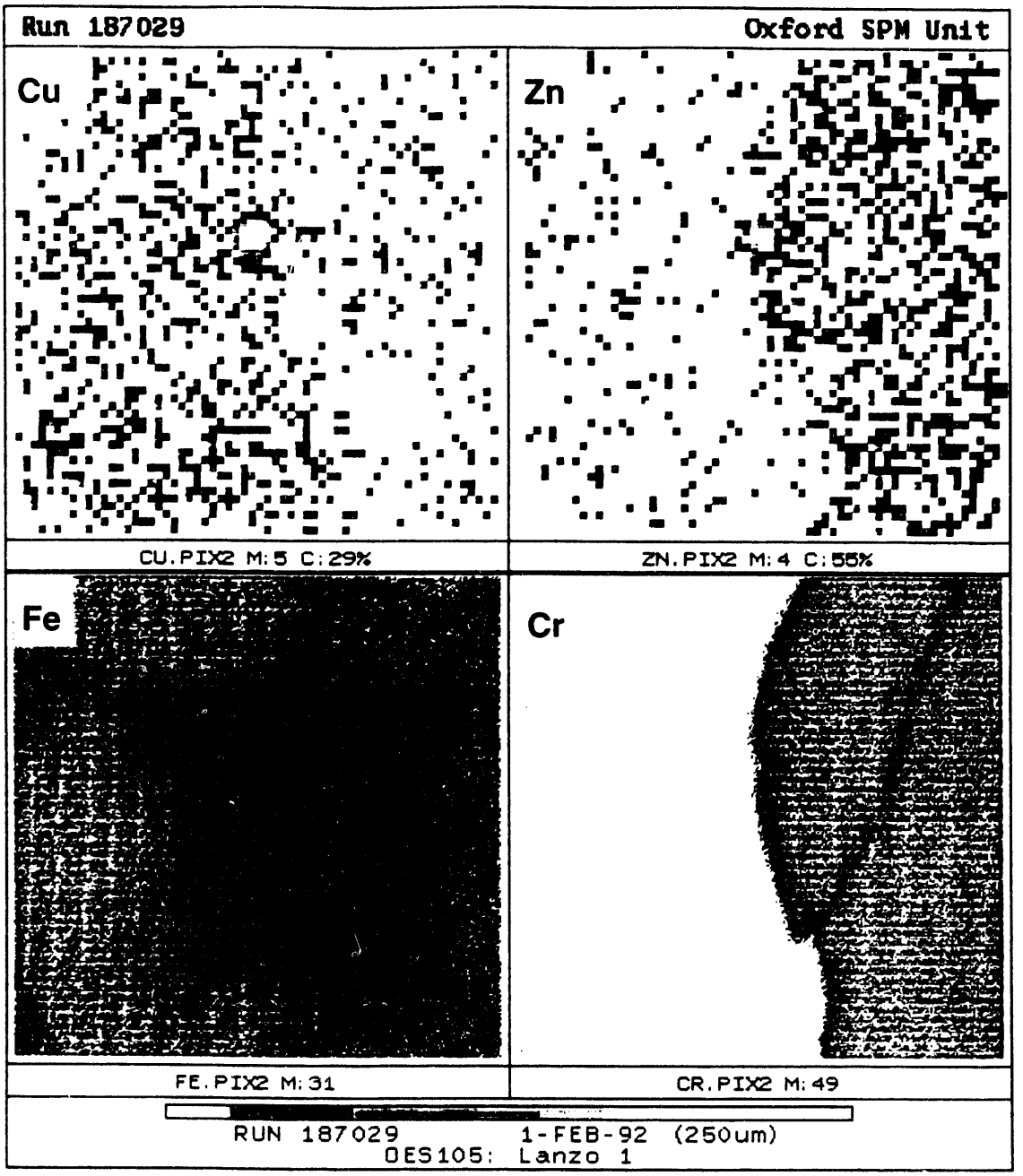
Run 187029
Oxford SPM Unit
Cu
Zn
CU.PIX2 M:5 C:29%
ZN.PIX2 M:4 C:55%
Fe
Cr
FE.PIX2 M:31
CR.PIX2 M:49
RUN 187029 1-FEB-92 (250um)
OES105: Lanzo 1

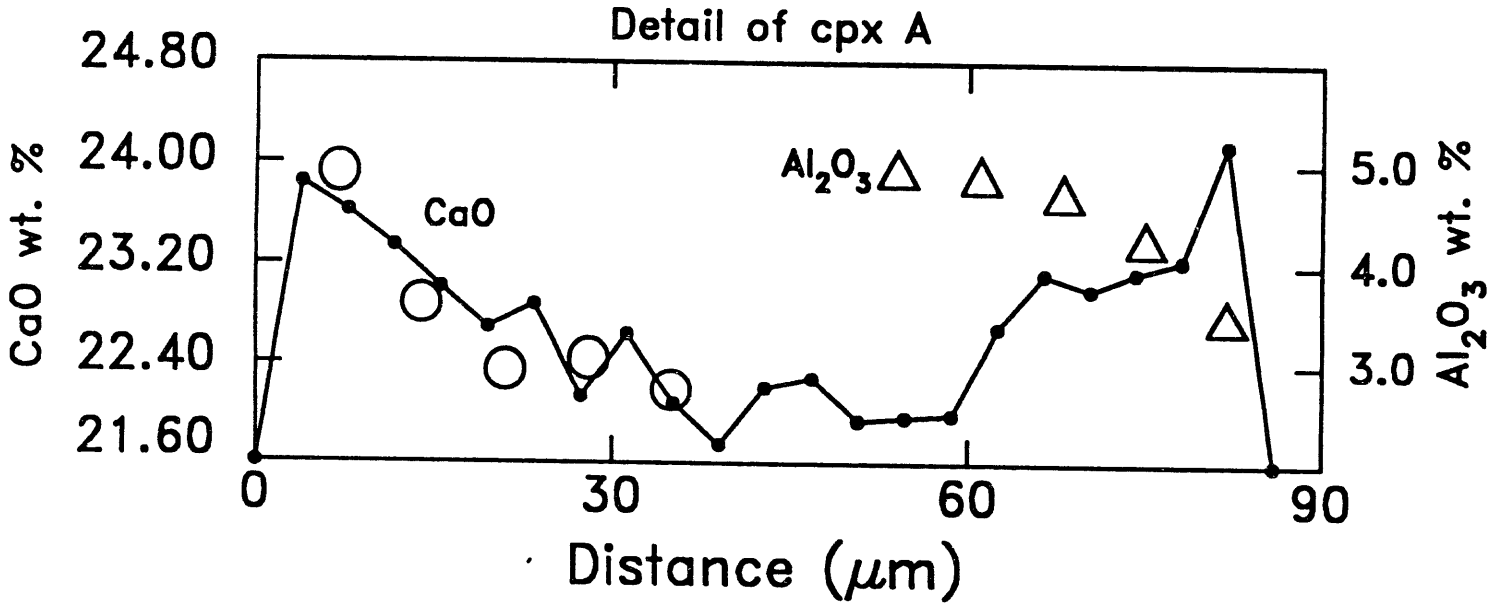
Detail of cpx A
24.80
24.00
23.20
22.40
21.60
CaO wt. %
CaO
Al_2O_3
5.0
4.0
3.0
Al_2O_3 wt. %
0
30
60
90
Distance (μm)

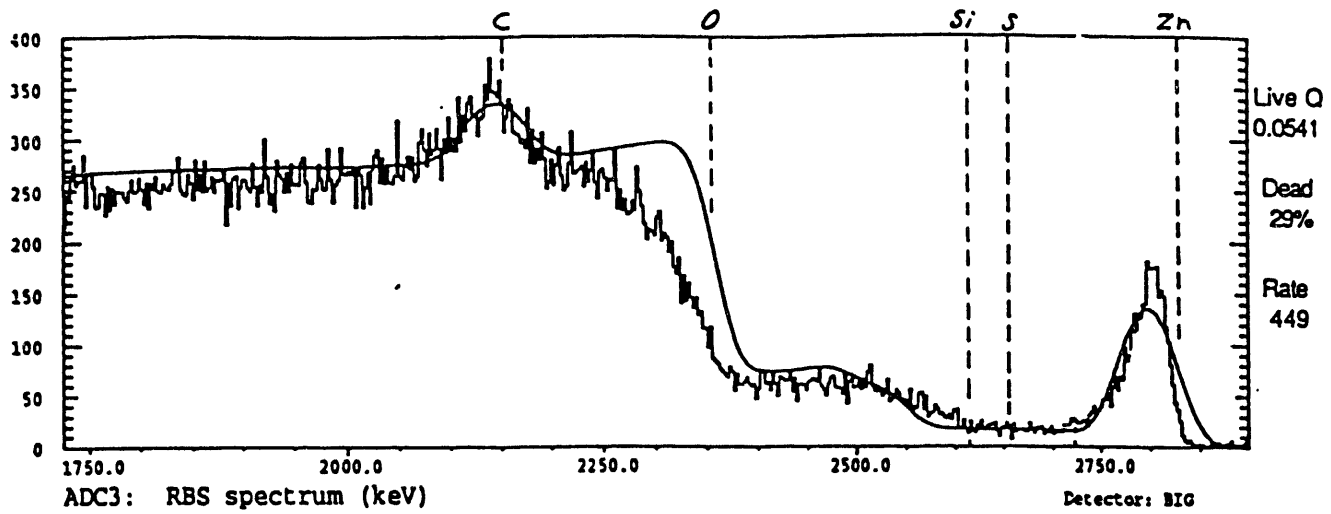
Run 187.030 OES105 Lanzo 1
t: 0:12:49 Beam Q: 0.0766uC
C
O
Si
S
Zn
400
350
300
250
200
150
100
50
0
Live Q
0.0541
Dead
29%
Rate
449
1750.0
2000.0
2250.0
2500.0
2750.0
ADC3: RBS spectrum (keV)
Detector: BIG

a

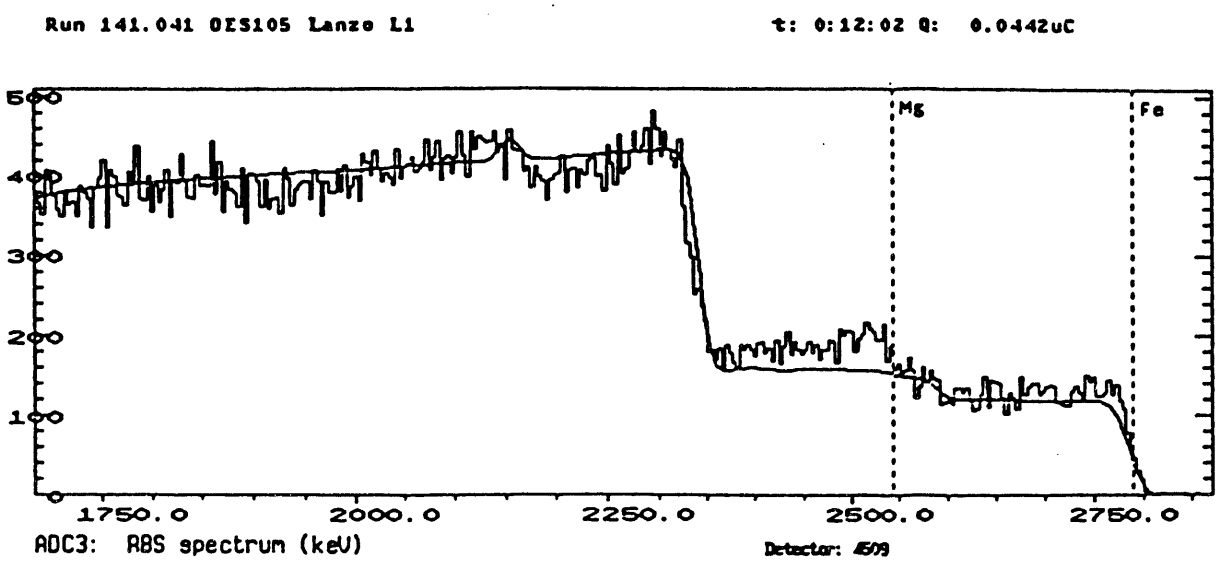
Run 141.041 OES105 Lanzo L1
t: 0:12:02 Q: 0.0442uC
500
400
300
200
100
Mg
Fe
1750.0
2000.0
2250.0
2500.0
2750.0
ADC3: RBS spectrum (keV)
Detector: 45/9

b.

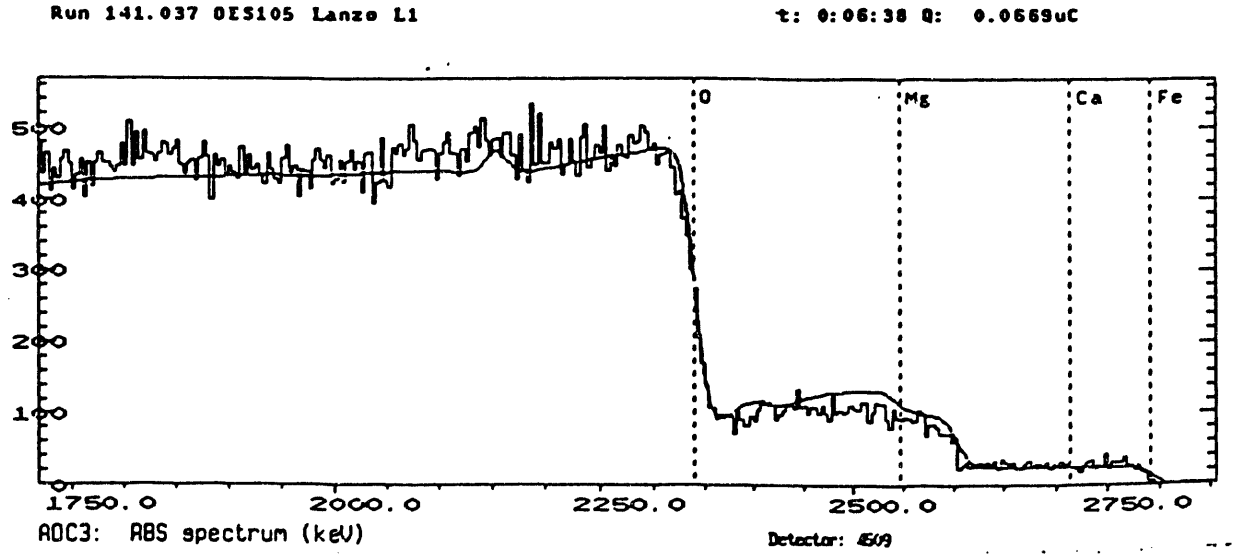
Run 141.037 OES105 Lanzo L1
t: 0:06:38 Q: 0.0669uC
500
400
300
200
100
O
Mg
Ca
Fe
1750.0
2000.0
2250.0
2500.0
2750.0
ADC3: RBS spectrum (keV)
Detector: 45/9

c.

Fig. (6)

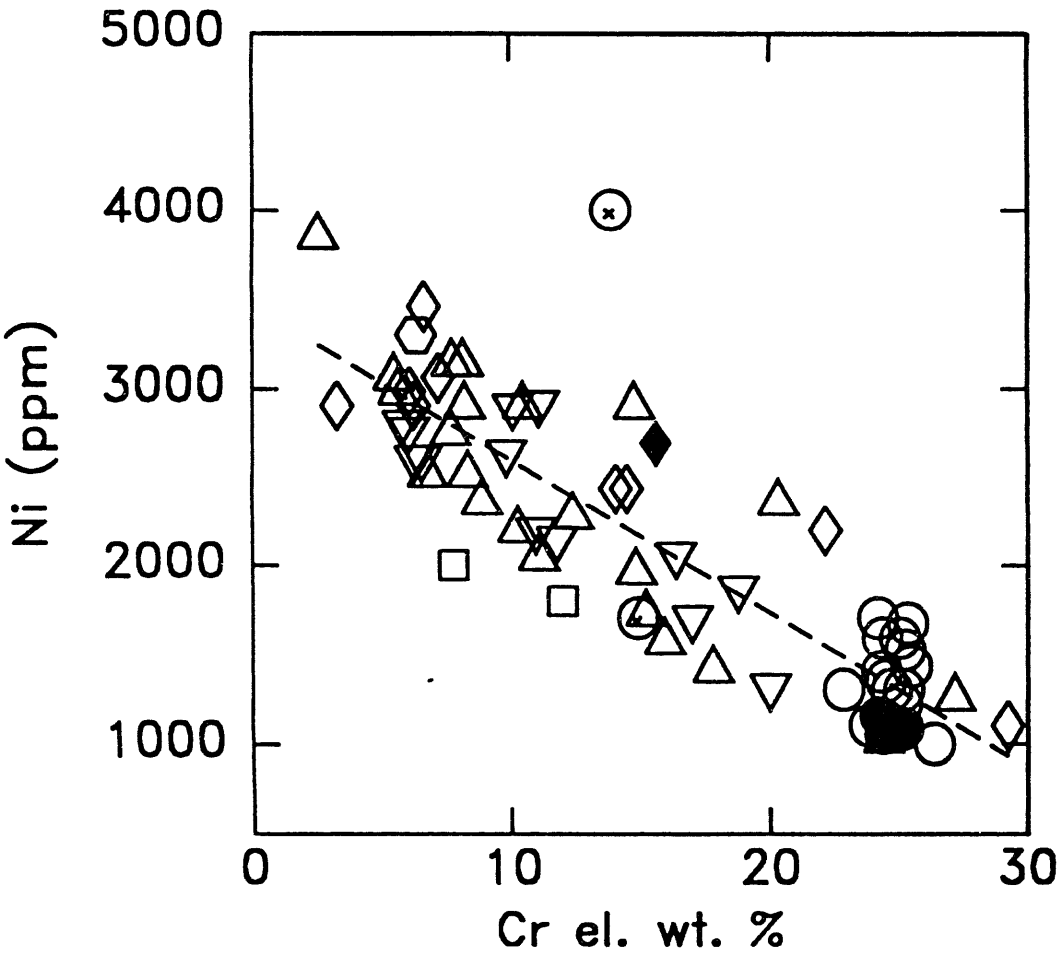

Fig 7

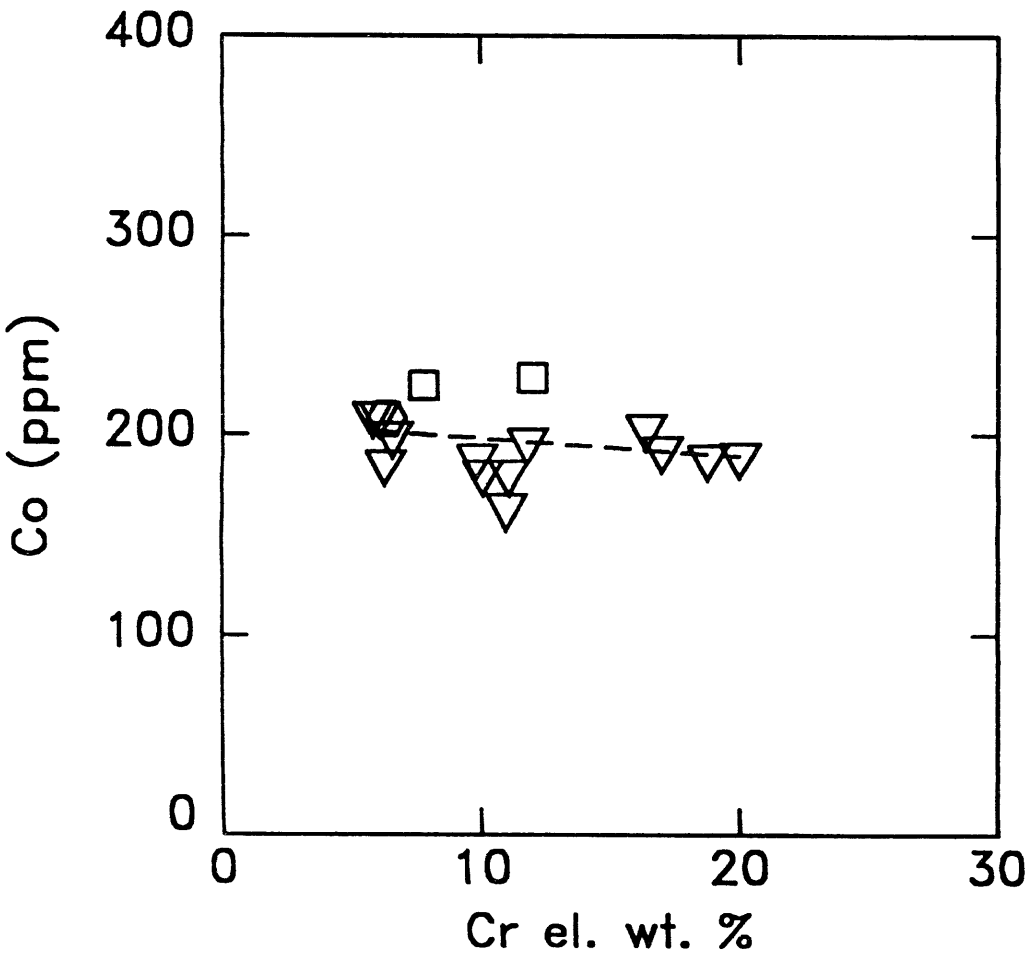

Fig 8

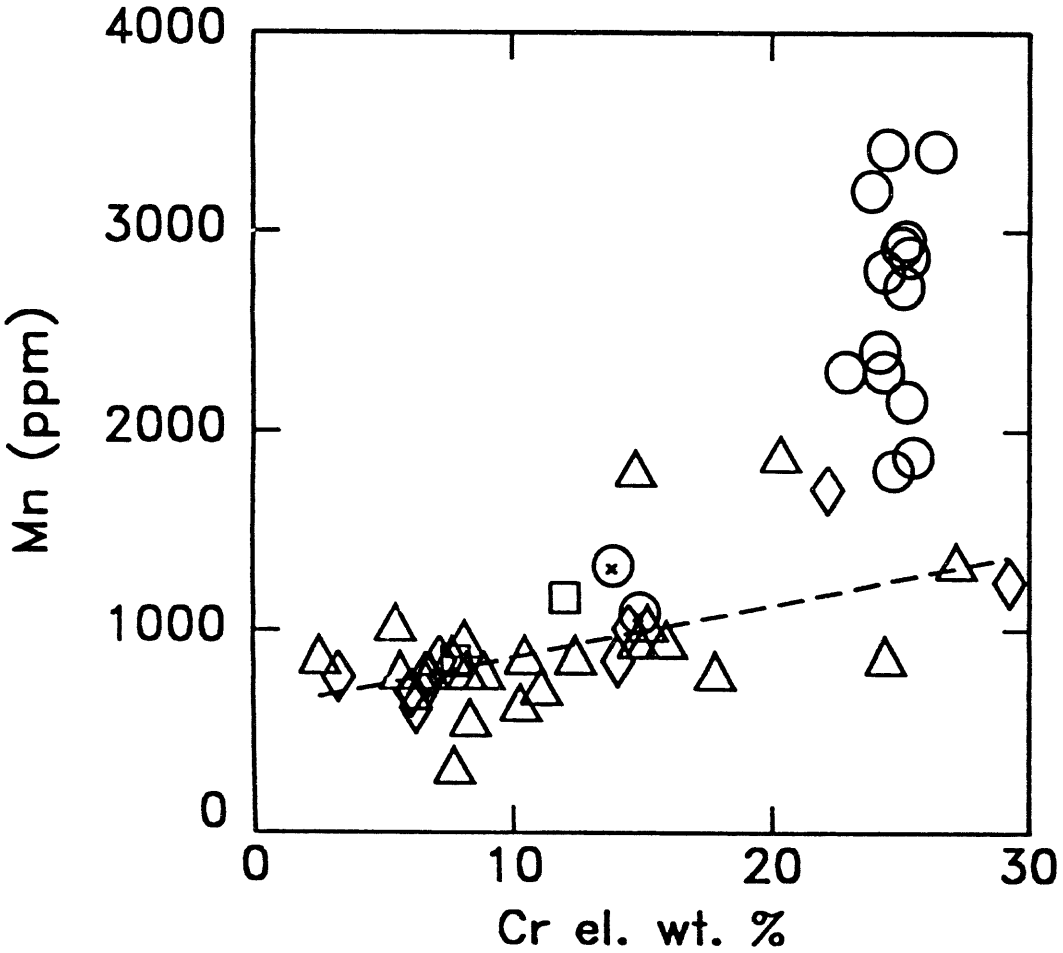

Fig 7

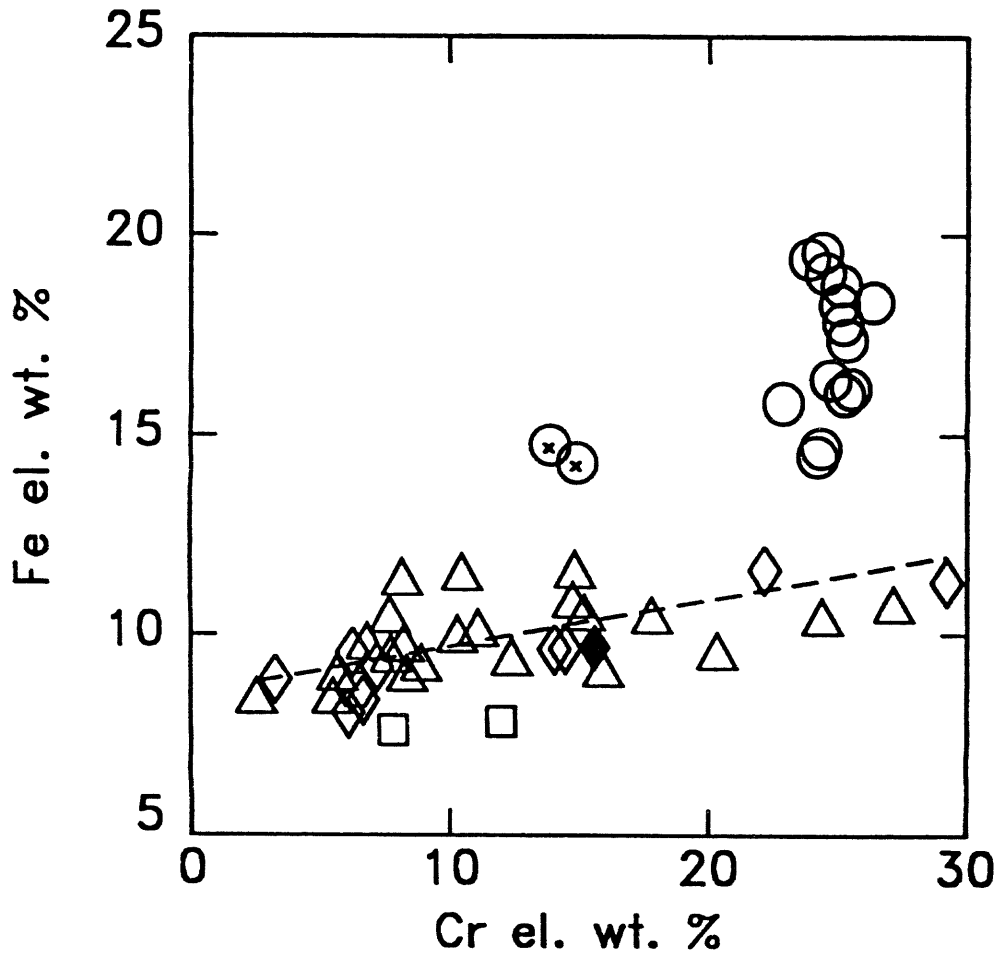

F.3 10

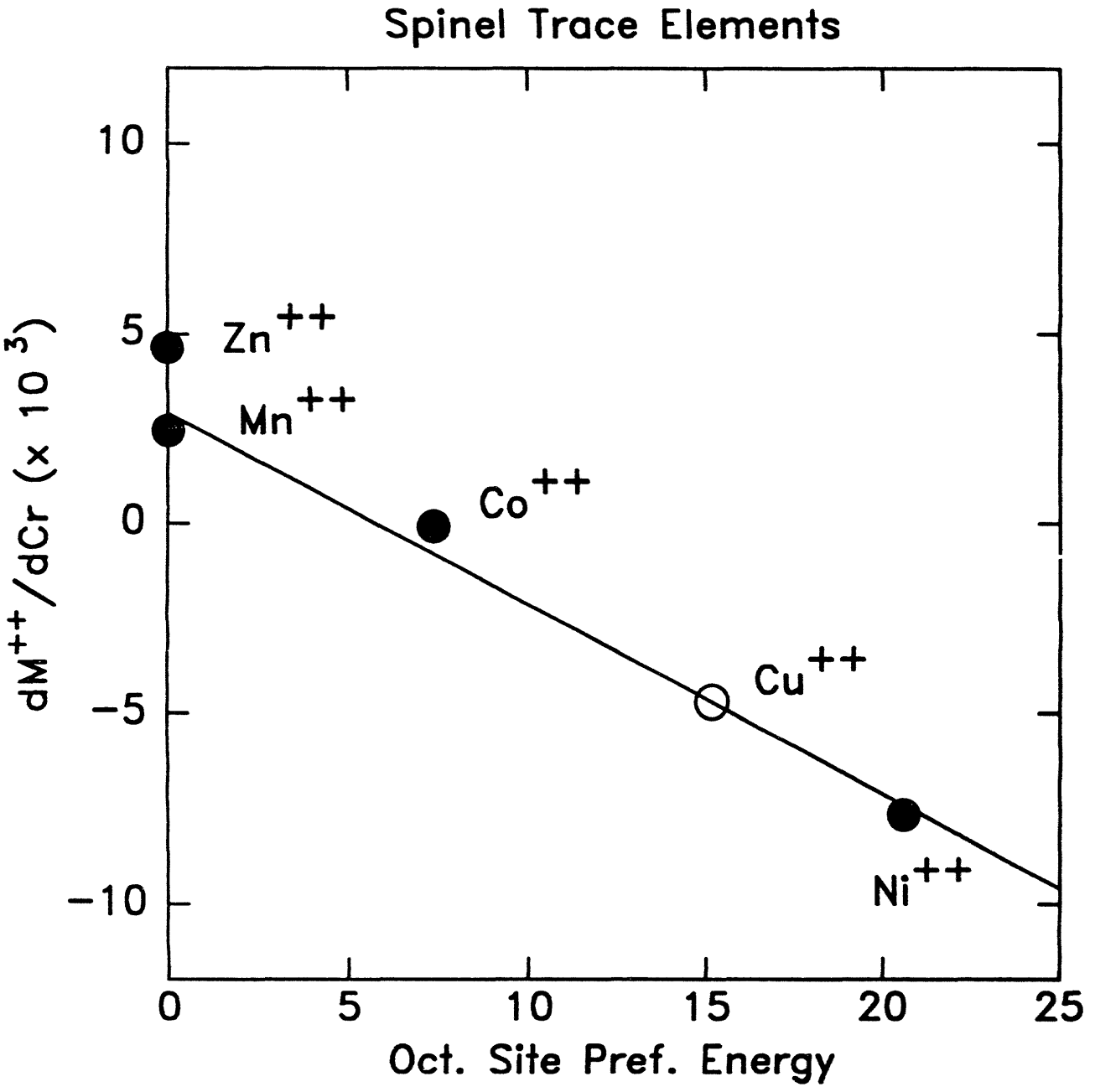
Spinel Trace Elements
10
5
0
−5
−10
0
5
10
15
20
25
dM++/dCr (x 10 3)
Oct. Site Pref. Energy
Zn++
Mn++
Co++
Cu++
Ni++

FIG. 11

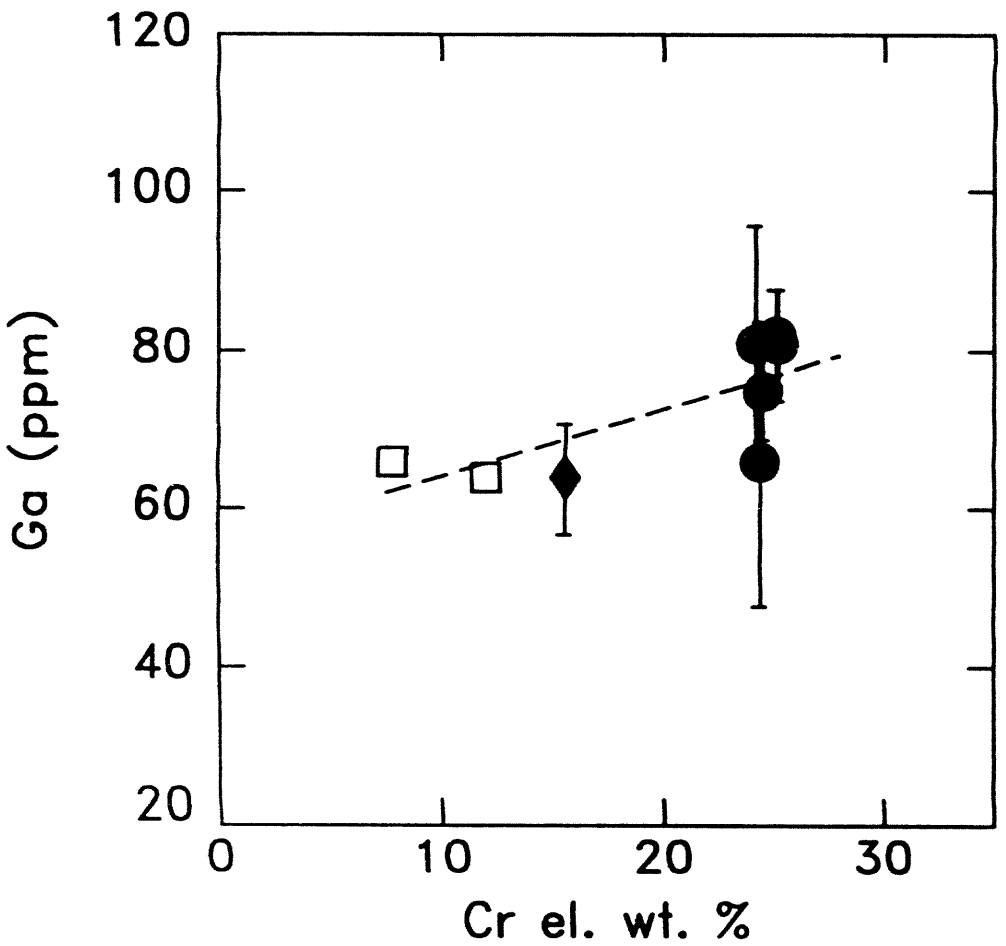

FIG. 12

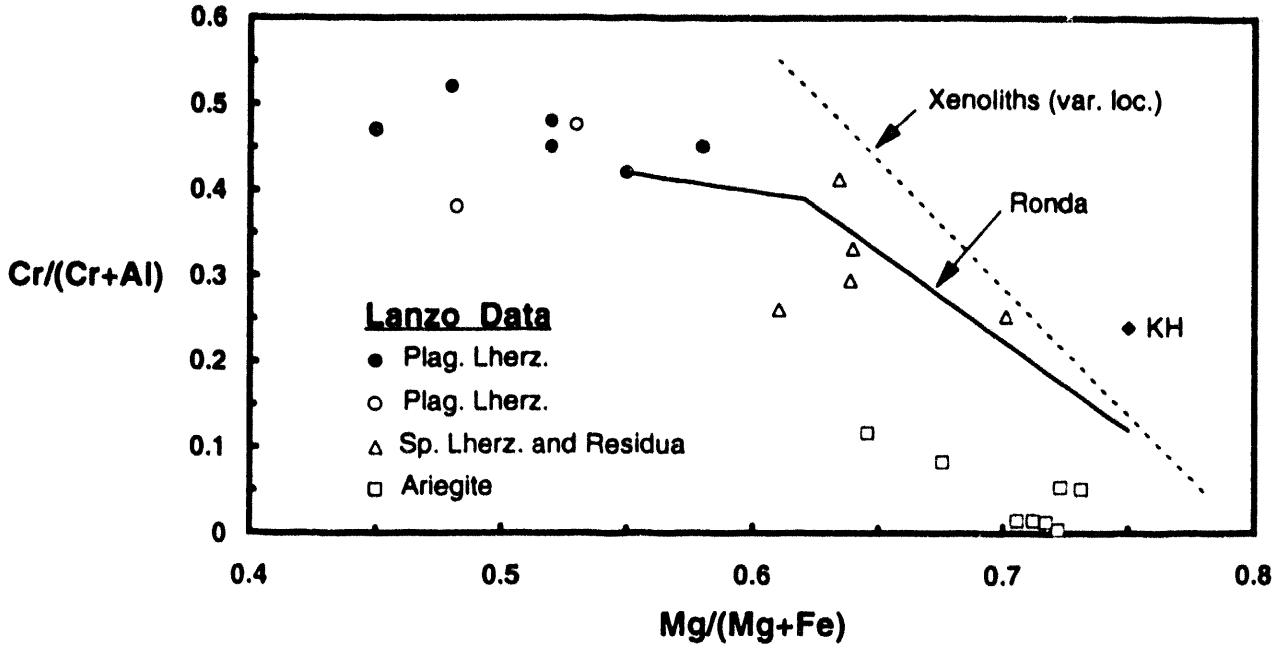
0.6
0.5
0.4
0.3
0.2
0.1
0
Cr/(Cr+Al)
0.4
0.5
0.6
0.7
0.8
Mg/(Mg+Fe)
Xenoliths (var. loc.)
Ronda
KH
Lanzo Data
Plag. Lherz.
Plag. Lherz.
Sp. Lherz. and Residua
Ariegite

FIG. 13

DATE
FILMED
6/23/94
END